PONTIFICIA UNIVERSIDAD CATÓLICA DE CHILE
ESCUELA DE INGENIERÍA

TOPOGRAPHICAL AND STRUCTURE-SOIL-STRUCTURE INTERACTION EFFECTS ON DYNAMIC BEHAVIOR OF SHEAR-WALL BUILDINGS ON COASTAL SCARP

JULIO CÉSAR SUCASACA RODRÍGUEZ

Informe de Actividad de Graduación para optar al Grado de
Magíster en Ingeniería Estructural y Geotécnica

Profesor Supervisor:
ESTEBAN PATRICIO SÁEZ ROBERT

Santiago de Chile, Abril, 2021.

A mi familia.

AGRADECIMIENTOS

Primeramente, deseo agradecer de manera especial al profesor Esteban Sáez a quien estimo bastante por ser una excelente persona, por su dedicada labor docente, y por su disposición y cordialidad siempre oportunas. Fue fundamental en el desarrollo de este trabajo, mediante su mentoría y retroalimentación. De quién aprendí bastante en mi formación en el emocionante mundo académico.

A los profesores de la escuela de Ingeniería Daniel Hurtado y Sergio Gutiérrez, por el apoyo, guía y motivación académica en temas profundos más allá del magister y por contagiar esa pasión por la enseñanza e investigación; y a los profesores Rafael Riddell y Jorge Vásquez P. por su impecable labor docente.

A mi familia, quienes me echaron de menos estos años, me animaron a continuar en esta aventura y me dieron soporte en los periodos complicados. Gracias por acompañarme.

Al personal administrativo del departamento de Ingeniería Estructural y Geotécnica, a la coordinadora Elena y Ana María, cuyo apoyo en estos años fue importante para el confortable desarrollo de las clases en el periodo de duración del magister.

A los compañeros y amigos con quienes compartí las salas de clase y de casa, quienes hicieron que este tiempo sea más ameno.

A la Sra. Elena, mi abuela chilena, quien me acogió con los brazos abiertos en todo momento desde el primer día de la estadía y motivó a concluir exitosamente este trabajo.

Al ingeniero Oscar Taiba, gerente de la empresa Ferrara, Proyectos Especiales, y al Msc. Dennis Raddatz, quienes amablemente compartieron los antecedentes y detalles del caso de estudio usado en este trabajo.

Al lector, quién hace que tenga sentido escribir con esmero este trabajo.

Finalmente, agradezco al programa Nacional de Becas y Crédito Educativo del gobierno peruano (PRONABEC), que mediante la Beca Presidente de la República, financió mis estudios de postgrado y permitió esta excelente experiencia académica y profesional.

INDICE GENERAL

Pág.

INDICE DE TABLAS

Pág.

INDICE DE FIGURAS

Pág.

RESUMEN

En este trabajo se investiga numéricamente la influencia de la topografía de talud, la estratigrafía del terreno y la interacción dinámica entre edificios próximos del tipo muros de corte de proyectos residenciales típicos ubicados en pendiente costera. Usando medidas de terreno, se calibró el modelo numérico de un edificio tipo tomado como caso de estudio. Se realizaron análisis dinámicos no lineales de elementos finitos para derivar factores de agravación topográfica previos a la excavación y construcción de los edificios, y para evaluar la respuesta estructural luego de la construcción de los edificios para diferentes escenarios y diferentes registros de movimiento del terreno. Se encontró que el perfil de la superficie del terreno tiene gran impacto en la respuesta dinámica de edificios pequeños y rígidos cuando sus longitudes de onda características son cercanas entre sí, y puede tener un rol perjudicial incrementando sobre 80% la deriva de entrepiso, 35% el coeficiente sísmico y 57% el periodo fundamental de base fija dependiendo de las señales de entrada. En muchos otros casos de señales de entrada que incluyen registros sísmicos de terremotos de campo lejano, la interacción dinámica suelo-estructura es beneficiosa. Además, se muestra que el escenario de estructura-suelo-estructura tiene efectos adicionales despreciables desde un punto de vista práctico respecto al escenario suelo-estructura para este caso de estudio. Estos resultados sugieren que proyectos residenciales similares deberían tener cuidado en el diseño de edificios pequeños ubicados cerca a la cresta del talud.

ABSTRACT

This paper investigates numerically the influence of slope topography, soil stratigraphy and dynamic interaction between close shear-wall buildings of typical residential projects on coastal scarp. A numerical model of reference real buildings taken as case of study is calibrated against field measurements. A nonlinear finite element dynamic analysis is conducted to derive topographical aggravation factors prior to excavation and construction of the buildings and to assess structural responses after their construction for different interaction scenarios and ground motion inputs. It is found the surface profile have large effect on the dynamic response of stiff low-rise building when their characteristic wavelengths are close each other and it can play a detrimental role increasing up to 80% the interstory drift, 35% the seismic coefficient and 57% the fixed-base fundamental period depending on the input. In several other input cases including far-field earthquake records, dynamic soil-structure interaction is beneficial. Furthermore, it is shown that structure-soil-structure scenario has negligible additional effect from a practical point of view with respect to soil-structure interaction for this case of study. These results suggest that similar residential projects should be cautious about the design of low-rise buildings located near a slope crest.

I. INTRODUCCIÓN

El permanente desarrollo de la economía y la sociedad, y el incremento del costo de las tierras conllevan a tener un acelerado crecimiento demográfico y un aumento progresivo de la necesidad de vivienda propia. Estas son situaciones que motivan la búsqueda de soluciones en muchas disciplinas tales como la ingeniería. En particular, en el rubro inmobiliario, para cubrir estas brechas de manera óptima, muchos proyectos residenciales son forzados a emplazarse en lugares desafiantes, con edificios más próximos entre sí, y con un requerimiento creciente en la cantidad de niveles. Un ejemplo de estos son los numerosos complejos habitacionales ubicados a lo largo del litoral costero entre las comunas de Valparaíso y Concón en Chile, que además se encuentran en una zona con un exquisito historial sísmico (Udias et al., 2012; Plafker and Savage, 1970; Comte et al., 1986).

Circunstancias similares a esta última implican tener que superar complicaciones en el diseño de estructuras de edificación que no suelen estar contempladas en los códigos de diseño sísmico vigentes. Sin embargo, la falta de entendimiento de estos problemas nos sugiere tener que prestarle la atención debida. Uno de estos problemas son los fenómenos que modifican la demanda sísmica en estas zonas con topografía del tipo talud costero. También la proximidad de los edificios genera incertidumbres sobre el comportamiento sísmico de estas estructuras.

En la actualidad, la mayoría de los códigos de diseño sísmico en el mundo contemplan únicamente modelos de estructuras de base fija, y ninguno de los problemas anteriores son tomados en consideración, pese a que sus efectos podrían ser determinantes en el correcto diseño sísmico. El propósito de este trabajo es evaluar la influencia de los efectos topográficos y la interacción dinámica no-lineal estructura-suelo-estructura en la respuesta

dinámica de edificaciones típicas chilenas de muros de corte ubicados sobre talud costero de suelo arenoso a través de modelos numéricos calibrados de un caso de estudio representativo.

I.1 Motivación

La principal motivación de este estudio es la falta de reglamentos que consideren adecuadamente los efectos topográficos de perfiles de superficie del tipo talud costero arenoso en el análisis y diseño de edificaciones residenciales ubicadas cerca de la cresta del talud, tales como muchos proyectos residenciales ubicados en el litoral costero entre Valparaíso y Concón en la región de Valparaíso en Chile.

I.2 Hipótesis

Los efectos topográficos y la interacción dinámica estructura-suelo-estructura (SSSI) tienen un rol fundamental en la respuesta dinámica de edificaciones residenciales típicas chilenas de muros de corte ubicadas cerca de la cresta del talud costero arenoso. Estos efectos pueden ser evaluados usando modelos numéricos calibrados de elementos finitos que consideran simultáneamente los dominios del suelo y de la estructura, además del comportamiento no lineal del suelo.

I.3 Objetivos

El propósito de este estudio es evaluar la influencia de los efectos topográficos y la interacción dinámica no-lineal estructura-suelo-estructura (SSSI) en la respuesta dinámica de edificaciones típicas chilenas de muros de corte ubicados sobre talud costero de suelo arenoso a través de modelos numéricos calibrados. Los objetivos específicos son los siguientes:

- Seleccionar un caso de estudio representativo de edificaciones residenciales típicas chilenas de muros de corte ubicadas sobre un talud costero, con información suficiente para el desarrollo de los modelos numéricos.
- Desarrollar los modelos numéricos completos 3D de base fija de los edificios del caso de estudio para calibrar modelos equivalentes 2D.
- Desarrollar y calibrar el modelo numérico completo de suelo y estructuras.
- Evaluar los efectos topográficos mediante análisis de propagación de ondas sísmicas planas verticales sobre el talud costero y el perfil superficial excavado previo a la construcción de los edificios.
- Evaluar los efectos de interacción dinámica no-lineal estructura-suelo-estructura en la respuesta de las edificaciones y compararlos con los casos de base fija.

I.4 Revisión de literatura

I.4.1 Propagación de ondas

En matemáticas y física, una onda es una perturbación dinámica que se propagan a partir de una fuente transportando energía y se idealiza mediante la ecuación de onda. Las ondas mecánicas, como por ejemplo las ondas sísmicas, se propagan en una dirección 3D desde una fuente sísmica y a través de un medio físico como el suelo al interior de la tierra, esta propagación es de partícula a partícula y va generando esfuerzos y deformaciones locales en el medio. En su recorrido, el frente de onda de una onda monocromática puede reflejarse, refractarse, atenuarse y cambiar de frecuencia.

Una simplificación usual cuando la fuente es lejana, es considerar ondas planas, donde las perturbaciones son idénticas a lo largo de un plano infinito perpendicular a la dirección de propagación de la onda. Sin embargo, cuando la fuente es cercana, esta simplificación no es válida.

De acuerdo a las cinemáticas asociada a las soluciones de la ecuación de onda, las ondas se clasifican en ondas de cuerpo y superficiales. Las ondas de cuerpo son de dos clases: ondas "P" con polarización[1] paralela a la dirección de propagación del frente de onda, y ondas "S" con polarización contenida en el plano del frente de onda. Esto se observa en la Figura I-1. Las ondas "S" se descomponen en su componente horizontal "SH" y la componente perpendicular "SV". Cuando el frente de onda plana tiene dirección vertical, ambas componentes "SH" y "SV" tienen polarización horizontal.

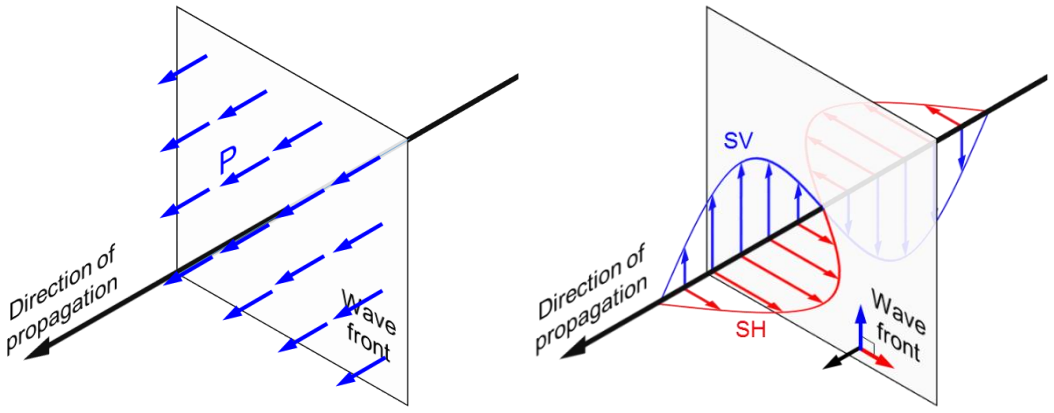

Figure I-1. Ondas de cuerpo "P" y "S" y sus direcciones de polarización.

[1] La polarización o dirección de polarización se refiere a la dirección de movimiento de las partículas del medio perturbado cuando una onda se propaga.

Las ondas superficiales corresponden a soluciones con componentes imaginarias de la ecuación de onda que se caracterizan por viajar a lo largo de la superficie del medio o una interfaz de gran contraste de impedancia, y por tener un decaimiento exponencial en profundidad como las ondas de Rayleigh, Love, Stoneley, etc, como se muestra en la Figura I-2. Estas ondas son también en parte responsables del daño en estructuras cuando se trata de eventos sísmicos.

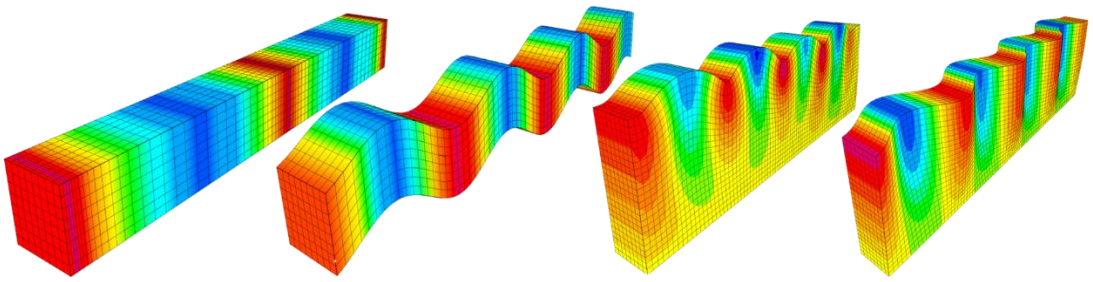

Figura I-2. De izquierda a derecha: Ondas de cuerpo “P”, y “S”; y ondas superficiales de Rayleigh y de Love.

Si bien existen abundantes soluciones fundamentales para la ecuación de la elasto-dinámica (Kausel, 2006), que es la forma elástica y lineal de la ecuación de onda de la mecánica, la forma general de esta ecuación puede resolverse mediante métodos numéricos (ver Sección I.4.4), capaces de reproducir comportamientos complejos. Esto es útil cuando se tienen suelos heterogéneos, geometrías superficiales complejas y cargas dinámicas complejas.

I.4.2 Interacción suelo-estructura

En términos sencillos, la interacción suelo estructura (SSI) estudia la respuesta dinámica acoplada de una estructura que es interdependiente con la respuesta del suelo

sobre el que está fundada. Este fenómeno también puede interpretarse como los efectos de la propagación de ondas ($\ddot{u}$) sobre los dominios del suelo (Ω_{soil}) y estructural (Ω_{st}), los que se encuentran acoplados mediante la interfaz entre ambos dominios (Σ) (Figura I-3). Además, la resolución numérica de este fenómeno requiere truncar el dominio computacional a través de una frontera artificial adecuada (Σ_{RC}) que cumpla la condición de radiación (Wolf, 1985), permitiendo que las ondas no sean retenidas en este dominio computacional.

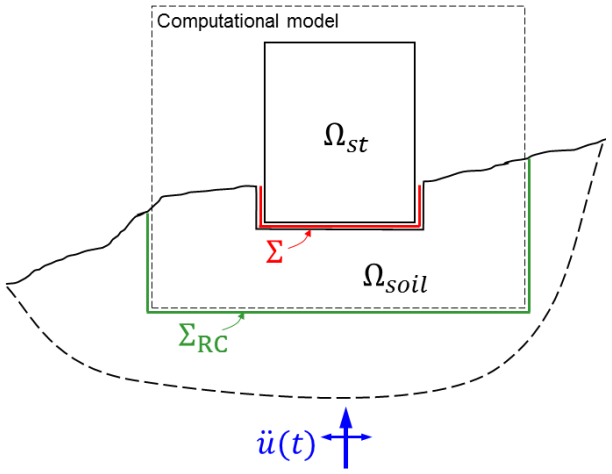

Figura I-3. Definición de dominios del suelo y la estructura.

El fenómeno de SSI es interdisciplinario y su evaluación rigurosa requiere que se estudien varios aspectos como el riesgo sísmico, la topografía, la heterogeneidad del sitio, el nivel freático, el comportamiento no lineal cíclico del suelo, características no lineales de la estructura y la interacción dinámica con otras estructuras (Sáez, 2009). Sin embargo, no todos los métodos de análisis pueden considerar estas características. Existen soluciones analíticas y numéricas para casos estáticos y dinámicos de interacción suelo-estructural cuya evolución histórica se encuentra bien documentada

en Kausel (2010), Menglin et al. (2011) y Roesset (2013). Los métodos de subestructura son rigurosos para problemas lineales y consisten en resolver independientemente cada dominio dividiéndo los efectos completos de SSI en los efectos de la interacción cinemática e inercial a través del uso de funciones de transferencia y de impedancia en el dominio de la frecuencia o del tiempo (Wolf, 1985, 1988), estos métodos fueron ampliamente usados en la década de los 80's. Sin embargo, para otros casos, los métodos directos que incluyen ambos dominios de forma explícita haciendo uso de métodos numéricos como elementos finitos (Zienkiewics et al., 1999), son adecuados porque pueden considerar no linealidades, geometrías complejas y el desarrollo de presión de poros. Estos métodos directos permiten evaluar la modificación de las características de la excitación dinámica en la base del edificio respecto a un movimiento teórico de campo libre, pero a expensas de mayor costo computacional.

I.4.3 Modelo constitutivo de suelo

Los modelos constitutivos describen la respuesta de materiales cuando son perturbados por acciones externas (cargas mecánicas, térmicas, etc), y deben cumplir con los principios de determinismo, acción local, segunda ley de la termodinámica, objetividad y simetría. (Tadmor et al. 2012)

En el caso del suelo, el modelo más sencillo es el uso de la ley de Hooke generalizada que asume al suelo como un sólido continuo, lineal, elástico, homogéneo e isótropo. Modelos más avanzados se fundamentan en observaciones fenomenológicas bajo el concepto de teoría de plasticidad (De Souza Neto et al., 2011; Simo and Hughes, 2006). Uno de estos modelos es el modelo de Mohr-Coulomb (MC) que idealiza al

suelo como un material elasto-plástico perfecto que no es capaz de reproducir endurecimiento (*hardening*), ablandamiento (*softening*) ni cambio volumétrico irreversible en trayectorias isotrópicas.

El modelo de endurecimiento de suelo (HSM), desarrollado por Schanz (1999) es una mejora al modelo MC, y adapta la idea de modelos hiperbólicos al contexto de la teoría clásica de plasticidad. Este modelo de pequeñas deformaciones se caracteriza por tener endurecimiento debido a distorsión de corte plástico y deformación volumétrica; rigideces de carga virgen, recarga y descarga dependientes del confinamiento; incluye comportamiento de dilatancia o contractancia del suelo; y tiene parámetros que se calibran con ensayos triaxiales y edométricos convencionales.

Este modelo fue extendido en la tesis doctoral de Benz (2007) para representar el comportamiento del suelo ante amplitudes cíclicas de deformación muy pequeñas dentro del rango elástico incorporando la degradación de la rigidez y el incremento del amortiguamiento de pequeña deformación, y es conocido como el modelo de endurecimiento de suelo con rigideces a pequeña deformación (HS small).

Las características del modelo HS small hacen que sea ideal para idealizar el comportamiento de suelos arenosos ante carga estática y cíclica como los usados en el caso de estudio de este trabajo.

I.4.4 El método de elementos finitos en geotecnia

El comportamiento estático y dinámico de medios porosos que contienen fluido, tal como el suelo, está gobernado por ecuaciones de campo correspondientes a la conservación de la masa, el balance del momento lineal y la conservación de la energía (Zienkiewicz et al. 1999) que junto a las ecuaciones de las relaciones constitutiva, las

condiciones de borde y las condiciones iniciales, proveen un *set* completo de ecuaciones e incógnitas. El método de elementos finitos es un método numérico que se usa para discretizar el dominio o dimensión espacial de estos sistemas de ecuaciones diferenciales en derivadas parciales haciendo uso de *sets* de funciones de forma y de incógnitas. Lo que finalmente conlleva a la obtención de sistemas de ecuaciones algebraicas aproximados al problema original que pueden ser resueltas con métodos numéricos más convencionales.

La formulación acoplada del tipo u-p (Zienkiewicz et al. 1999) permite resolver problemas dinámicos de baja frecuencia como el caso típico de carga sísmica no impulsiva, y problemas de consolidación estáticos drenados o no drenados típicos de la mecánica de suelos.

En suma, la versatilidad y simplicidad del método de elementos finitos permite considerar múltiples dominios con geometrías complejas y relaciones constitutivas no lineales para el esqueleto sólido del suelo en el análisis dinámico de modelos directos de interacción suelo-estructura.

I.5 Metodología

Para estudiar la influencia de los efectos topográficos y la interacción dinámica no-lineal estructura-suelo-estructura en la respuesta de edificaciones, este trabajo consideró la creación de modelos numéricos elementos finitos de un caso de estudio representativo de edificaciones típicas chilenas de muros de corte ubicados en ladera costera arenosa, sobre los que se evaluaron múltiples escenarios. Las siguientes subsecciones detallan las técnicas y procedimientos sistemáticos usados en este trabajo. Primeramente, se presenta una revisión general del caso de estudio y la

estrategia metodológica general. Luego, se detalla el procedimiento de calibración dinámica de los modelos estructurales del caso de estudio; y la creación y calibración del modelo de interacción suelo-estructura. Seguidamente se presentan los escenarios considerados. Finalmente se explica el análisis espectral de las señales como forma de interpretación de resultados.

I.5.1 Caso de estudio y estrategia general

Se seleccionó un proyecto residencial típico de apartamentos ubicado en talud costero arenoso ubicado en el litoral costero entre Valparaíso y Concón en la región de Valparaíso de Chile. Este caso de estudio es representativo de los numerosos proyectos de vivienda con características similares presentes en esta zona urbana de alto riesgo sísmico. El talud costero arenoso tiene una pendiente promedio de 30° y una altura aproximada de 90 m. El edificio alto de apartamentos tiene 28 niveles y se ubica cerca del medio del talud con vista hacia el mar, y el edificio bajo de estacionamientos de 8 niveles está ubicado detrás del edificio de apartamentos cerca a la cresta del talud. Ambos edificios están estructurados con muros de concreto armado típicos chilenos (Westenenk, 2013) y están conectados con corredores.

A través de una colaboración con empresas privadas, se tuvo acceso a los detalles arquitectónicos y estructurales de la construcción de los edificios mostrados en la Figura I-4, al detalle del sistema de contención de tierras usado para contener las excavaciones de hasta 15.5 m de altura, a datos experimentales de instrumentación con inclinómetro durante el proceso constructivo, ensayos de extracción a tracción de micropilotes, y a la investigación geotécnica del proyecto. Además, se caracterizó el material superficial usando equipo triaxial (parámetros de resistencia) y el equipo de

torsión cíclica y columna resonante (curvas de degradación cíclica de rigidez y amortiguamiento)

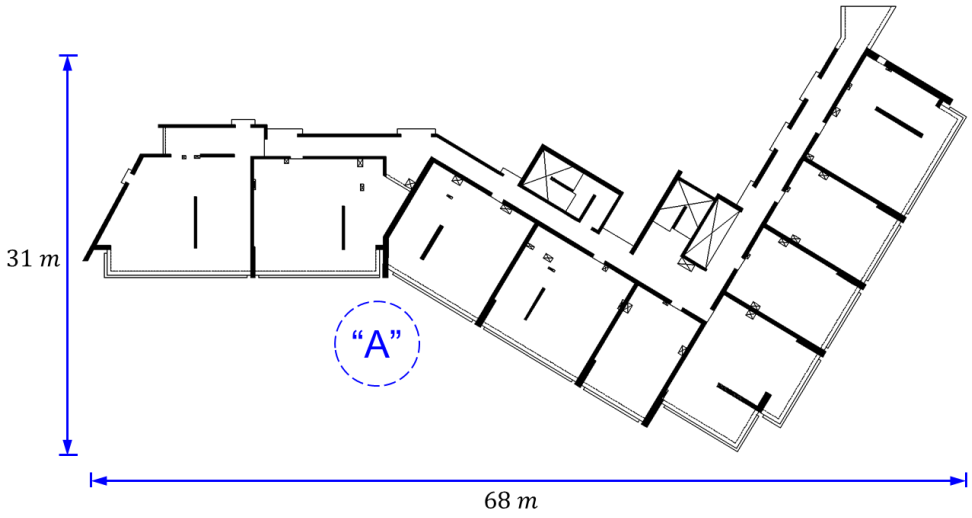

(a)

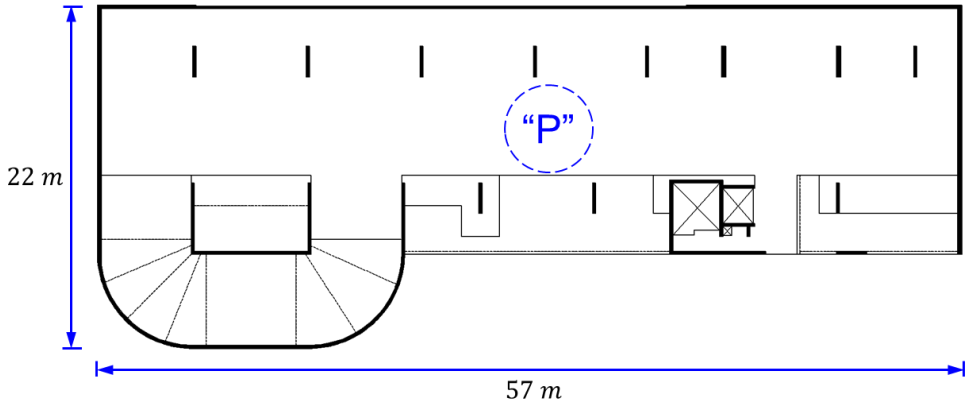

(b)

Figure I-4. Vista en planta de los edificios considerados como caso de estudio. (a) Edificio residencial. (b) Edificio de estacionamientos.

A partir del caso de estudio seleccionado, este trabajo consideró la creación de modelos numéricos completos 3D de las edificaciones, estos modelos se usaron para calibrar

dinámicamente modelos 2D equivalentes de deformaciones planas. Posteriormente, se desarrolló un modelo de elementos finitos completo que considera mutuamente los dominios de suelo y dominios estructurales, que se calibró estáticamente usando datos experimentales del sitio y de la construcción. Se realizaron análisis de propagación de ondas para varias geometrías del talud y análisis dinámicos no lineales para tres escenarios. Para estos análisis se usaron señales de entrada sintéticas del tipo Ricker con diferentes amplitudes y frecuencias centrales; y registros sísmicos de roca asociados a eventos compatibles con los esperados para la zona de estudio. Finalmente, los resultados de esfuerzos y deformaciones dependientes del tiempo se analizaron principalmente en el dominio de frecuencias usando relaciones espectrales e indicadores de fuerzas y desplazamientos.

I.5.2 Modelos y calibración

Usando la información disponible del caso de estudio, se desarrollaron modelos de elementos finitos usando *software* ampliamente conocido de análisis estructural y de análisis geotécnico. Estos modelos se calibraron como se detalla a continuación.

a) Modelos estructurales

Se realizaron modelos numéricos elásticos de los edificios de base fija usando elementos finitos del tipo *frame* y *shell*, los que se muestran en la Figura I-5. Se llevaron a cabo análisis de vibración libre para determinar las formas modales, y frecuencias de vibración natural que fueron usadas como referencia para calibrar modelos simplificados 2D. Estos modelos 2D fueron seleccionados a partir del eje estructural representativo del edificio más cercano a la sección transversal del talud

costero, y con un espesor unitario (1 m), de manera que fueran capaces de representar al modelo 3D en términos de masa sísmica, forma modal y frecuencias de vibración.

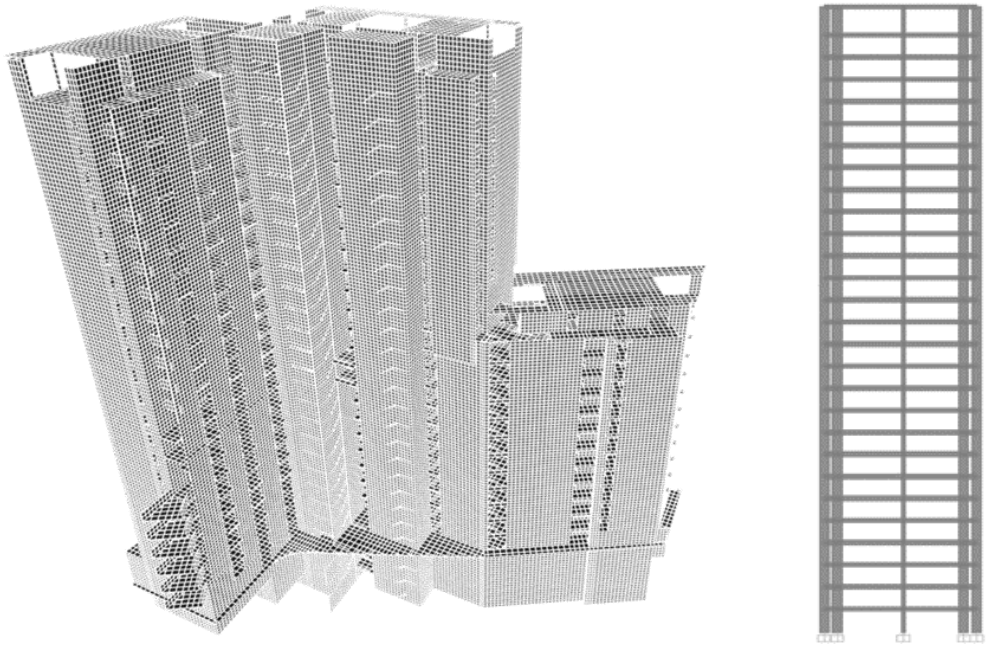

(a)

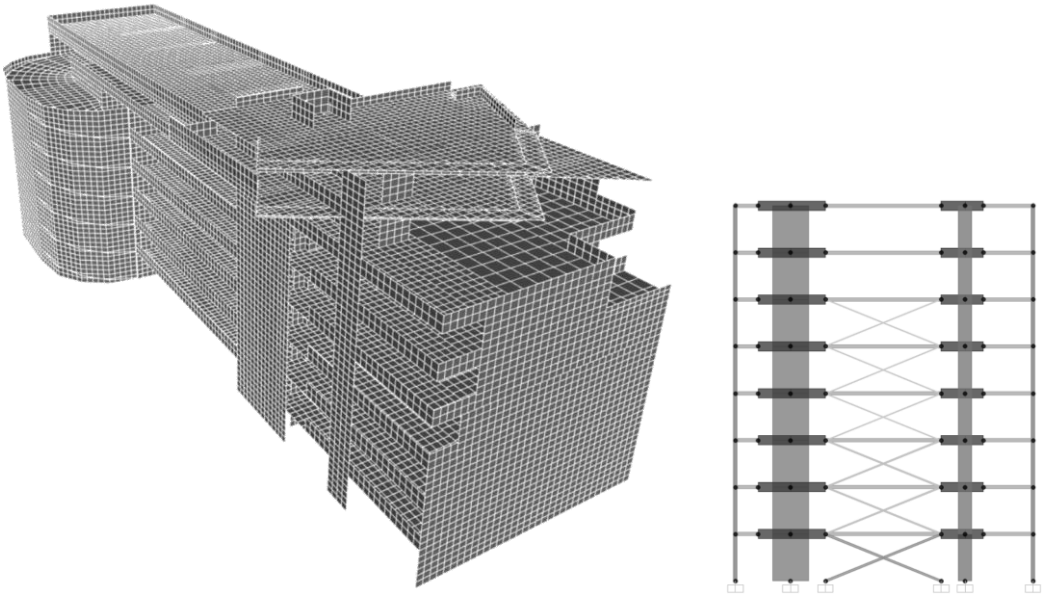

(b)

Figure I-5. Modelos de elementos finitos 3D y modelos equivalentes 2D. (a) Edificio residencial. (b) Edificio de estacionamientos.

Esta calibración se realizó mediante un proceso de optimización de rigideces definido de la siguiente forma.

$$\min_{\substack{s.t.\\ k_j>0}} \sum_{i=1}^{N=3} \left(A_1 \frac{\|\boldsymbol{\phi}_{3D} - \boldsymbol{\phi}_{2D}\|}{\|\boldsymbol{\phi}_{3D}\|} + A_2 \frac{|f_{3D} - f_{2D}|}{f_{3D}} \right) \tag{1.1}$$

Donde $\boldsymbol{\phi}$ es la forma modal normalizada y simplificada a un grado de libertad traslacional por nivel, $\boldsymbol{f}$ es la frecuencia natural de vibración del edificio para el modo $\boldsymbol{i}$, $\boldsymbol{A_1}$ y $\boldsymbol{A_2}$ son parámetros de pesos escalares, $\boldsymbol{k_j}$ es la rigidez del *j*-ésimo muro, y los subíndices "2D y 3D" hacen referencia a la dimensionalidad del modelo numérico.

La variable de diseño en la Ecuación (1.1) para el modelo 2D del edificio residencial de apartamentos es la rigidez de los cuatro muros idénticos extremos (medidos mediante sus espesores); mientras que para el modelo 2D del edificio de estacionamientos, son las rigideces de los muros centrales, extremos y diagonales en los primeros niveles. Se observó que los tres primeros modos de vibración son suficientes para el proceso de optimización.

b) Modelos de interacción suelo-estructura

Usando los modelos numéricos 2D equivalentes de los edificios, se elaboró un modelo de elementos finitos que incluye los dominios de suelo y estructurales con una malla no estructurada con al menos doce nodos a lo largo de la longitud de onda asociada a la máxima frecuencia de la señal de entrada. Este modelo representa la condición de

radiación en el borde del dominio computacional mediante fronteras de campo libre y tiene columnas de suelo adicionales que absorben las ondas salientes del modelo; las interfaces no lineales entre los dominios están basadas en el criterio de rotura de Mohr-Coulomb; y es capaz de representar el comportamiento inelástico del suelo mediante modelos constitutivos elasto-plásticos.

Se simuló secuencialmente las etapas constructivas de excavaciones, construcción de sistemas de contención de tierras, construcción de fundaciones y construcción de los edificios. El modelo se calibrado estáticamente, obteniéndose un buen ajuste numérico experimental en los perfiles de velocidad de la onda de corte, y en los perfiles de deflexión de una pila instrumentada del sistema de contención de tierras.

I.5.3 Escenarios considerados

Para evaluar la influencia de los efectos topográficos, se evaluó la propagación de ondas planas verticales en los siguientes escenarios crecientes en complejidad. (geometría de talud / modelo de suelo / estratos del suelo / señal de entrada)

- Casos idealizados.
    - Talud de baja pendiente, lineal, homogéneo, Ricker
    - Talud simplificado, lineal, homogéneo, Ricker.
    - Talud real, lineal, homogéneo, Ricker.
    - Talud real, lineal, estratificado, Ricker.
- Campo libre.
    - Talud real, no lineal, estratificado, Ricker 0.10g PGA.
    - Talud real, no lineal, estratificado, Ricker 0.40g PGA.
    - Talud real, no lineal, estratificado, registro UTFSM.
    - Talud real, no lineal, estratificado, registro RAPEL.
- Casos con excavación.

- Talud excavado, no lineal, estratificado, registro UTFSM.
- Talud excavado, no lineal, estratificado, registro RAPEL

Los escenarios para evaluar los efectos de interacción suelo-estructura fueron los siguientes:

- Edificios de base fija (sin interacción)
- Edificios individuales en base flexible. (interacción suelo-estructura) (solo la excavación y estructura de contención de tierras del edificio adyacente es considerado).
- Ambos edificios en base flexible (interacción estructura-suelo-estructura)

En todos los casos se usaron señales de entrada tipo Ricker con frecuencias centrales de 0.8, 1.5, 2.5 y 5.0 Hz para cubrir un rango de frecuencias entre 0.5 y 10 Hz donde los edificios, el sitio y el movimiento sísmico están contenidos; y los registros de aceleración no escalados en roca de los terremotos de Algarrobo (1985, comp. 70) y el Maule (2010, comp NS), medidos en la estación UTFSM y RAPEL respectivamente.

I.5.4 Análisis espectral

Los resultados de análisis dinámicos suelen presentarse como abundantes datos en series de tiempo, estos datos permiten extraer información útil de las respuestas de los dominios del suelo y estructural en función del tiempo. En adición, información más profunda en términos de contenido de frecuencias puede obtenerse mediante la descomposición de las series de tiempo estacionarias en sus componentes armónicas (representación en el dominio de frecuencias). Esto se realiza eficientemente a través de la transformada rápida de Fourier (Cooley and Turkey, 1965).

(a) Razones espectrales.

Para tener una mirada profunda a los efectos de la amplificación topográfica, inspirado en los trabajos de Apostolos et al. (1991) y Assimaki et al. (2005), en este trabajo se propone el factor de amplificación topográfica (TAF) para taludes como medida directa del potencial de amplificación topográfica. Este es una razón espectral que mide la amplificación relativa de las componentes armónicas de las series de tiempo y está definido de la siguiente forma:

$$TAF(x,f) = \frac{|\mathcal{F}\{\ddot{u}_x(x,t)\}|_{2D}}{|\mathcal{F}\{\ddot{u}_x(x,t)\}|_{1D}} \tag{1.2}$$

Donde x es la coordenada horizontal, f la frecuencia, $\ddot{u}_x(x,t)$ la aceleración horizontal del dominio del suelo en superficie, $|\mathcal{F}\{\cdot\}|$ es el módulo de la amplitud de Fourier de la serie de tiempo $\{\cdot\}$, y los subíndices 2D y 1D indican el modelo numérico.

De manera idéntica, para observar los efectos de la interacción suelo-estructura, se proponen dos razones espectrales que cuantifican la amplificación de las aceleraciones en los edificios y en la superficie del suelo entre varios escenarios en términos de frecuencias. En la Sección II.3.2 y II.3.3 se describen los detalles de las tres razones espectrales propuestas.

(b) Espectrogramas.

Usando la transformada discreta de Fourier de tiempo corto (Schafer and Rabiner, 1973) y una ventana de Hamming, se puede observar el contenido de frecuencia de las series temporales según avanza el tiempo en gráficos conocidos como espectrogramas (frecuencia vs tiempo). Esto se puede realizar para cada punto a lo largo de la

superficie del terreno para las amplitudes de Fourier de las componentes armónicas de una cantidad de respuesta como se observa en la Figura I-6. Este concepto propuesto en este trabajo es útil para entender cómo se propagan las componentes armónicas de del movimiento del terreno a lo largo de la superficie debido a acciones dinámicas y para comparar diferentes escenarios; por ejemplo, en la Figura I-7 se observa un instante de este gráfico (video) en el que se comparan dos escenarios.

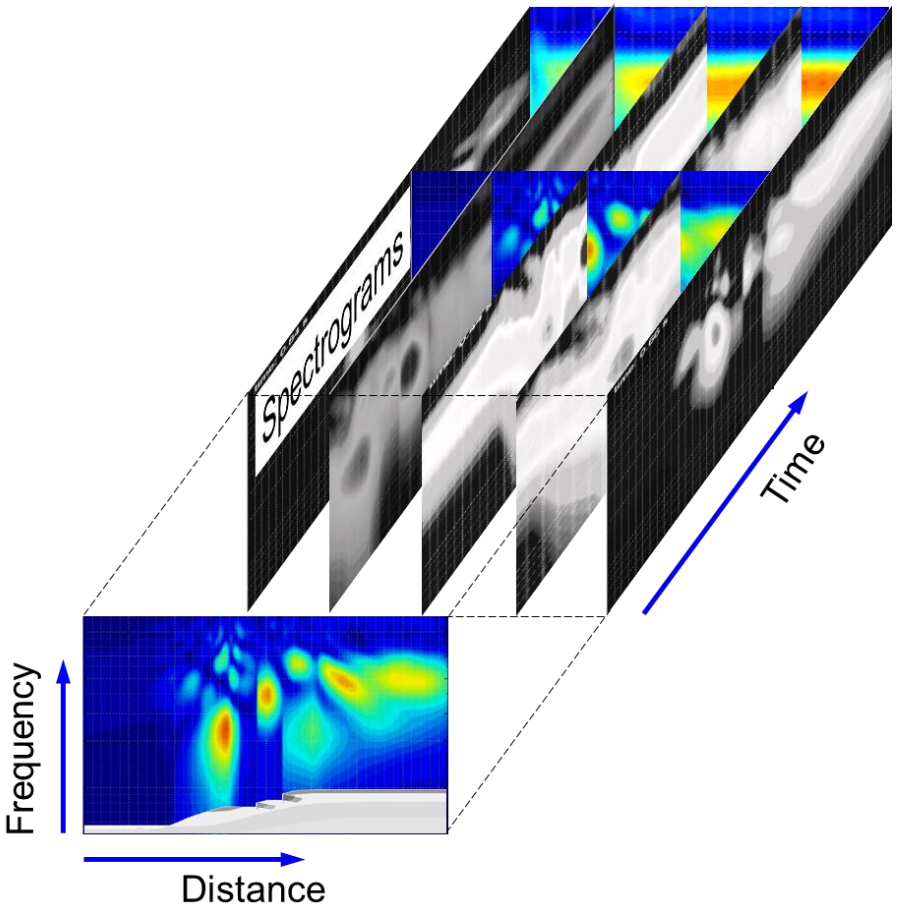

Figura I-6. Construcción de un gráfico distancia-frecuencia-tiempo para las amplitudes de Fourier para una determinada cantidad de respuesta (escala de colores) a lo largo de la superficie de terreno.

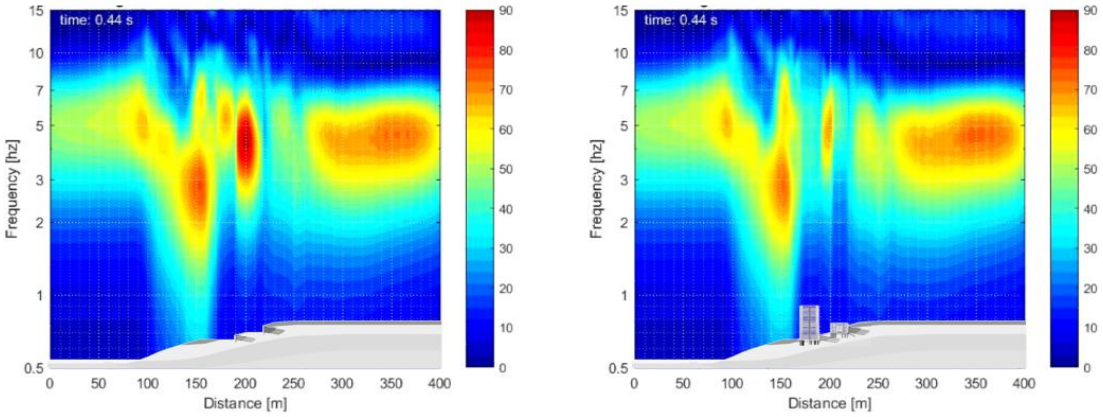

Figure I-7. Gráficos de distancia-frecuencia para un instante t=0.44s de la amplitud de Fourier de las aceleraciones horizontales inducidas por un pulso Ricker de 5.0 Hz de frecuencia central y una amplitud de 0.40g a nivel del afloramiento rocoso (a) Previo a la construcción del edificio. (b) Con ambos edificios.

I.6 Principales conclusiones

En este trabajo se estudió la influencia de los efectos topográficos y la interacción dinámica no-lineal estructura-suelo-estructura en la respuesta de edificaciones residenciales de muros de corte típicas de 28 y 8 niveles ubicadas cerca de la cresta de un talud costero arenoso. Para ello, se desarrollaron modelos numéricos calibrados de elementos finitos de deformaciones planas que incluyen los dominios del suelo no homogéneo y no lineal, y de ambas estructuras. Se realizaron análisis dinámicos no lineales usando señales de entrada sintéticas del tipo Ricker y registros sísmicos reales; y se analizaron las respuestas usando relaciones espectrales e indicadores de fuerzas y desplazamientos.

Para el caso de estudio evaluado, es decir, las características del sitio, de los edificios, y de las señales de entrada usadas en esta investigación, se derivaron las siguientes conclusiones.

- El perfil topográfico del talud natural, al igual que el perfil superficial excavado tienen gran influencia en los patrones de propagación de onda, pudiendo amplificar o disminuir el movimiento del terreno en determinadas zonas y para ciertas frecuencias. Además, este perfil superficial del terreno puede cambiar dramáticamente la cinemática del movimiento de edificios pequeños y rígidos.
- La estratigrafía del suelo puede modificar la dirección de propagación de las ondas planas verticales, amplificando o reduciendo el movimiento del terreno en la superficie.
- Las fundaciones profundas de los edificios intensifican la respuesta acoplada del suelo y la estructura; y tienden a disminuir la componente de aceleración vertical en superficie para las altas frecuencias.
- Considerar el análisis de interacción suelo-estructura (SSI) muestra que el modelo de base fija del edificio pequeño y rígido puede conllevar a predicciones no conservadoras de la respuesta estructural para algunas frecuencias centrales de las señales de entrada del tipo Ricker, mientras que para otras frecuencias, las respuestas predichas son conservadoras.
- Los efectos adicionales del análisis de interacción estructura-suelo-estructura (SSSI) sobre las respuestas estructurales son despreciables desde un punto de vista práctico.

- Interpretar los resultados en términos de frecuencia y longitud de onda nos brinda un entendimiento cuantitativo y más completo de los efectos topográficos y los efectos de interacción dinámica no-lineal suelo-estructura.
- Proyectos residenciales similares en taludes costeros deberían poner atención en el diseño de edificios pequeños ubicados detrás de una excavación profunda y cerca de la cresta del talud.

I.7 Trabajo futuro

En base a los resultados y el alcance de este trabajo, recomendaciones para trabajos futuros incluyen lo siguiente:

- Evaluar la influencia del ángulo de incidencia de la señal de entrada en el potencial de amplificación topográfica. La bibliografía sugiere que propagar ondas planas verticales podría no ser el caso más crítico cuando se tiene taludes y suelos estratificados, pues como se mostró en este trabajo, la estratigrafía modificará la dirección de las ondas propagadas, y podrían tenerse ángulos críticos de señales de entrada para lo cual la modificación es no conservadora.
- Evaluar el efecto del nivel freático superficial. El desarrollo de presiones de poros en el suelo ante solicitaciones sísmicas modificará su resistencia y rigidez y con ello la propagación de ondas y la interacción dinámica suelo-estructura de formas aún más complejas pero susceptibles a ser entendidas.
- Mejorar el modelo de la condición de radiación. Por ejemplo esquemas numéricos derivados de PML (*perfectly matched layer*) se comportarían mejor que los enfoques usados en este estudio, y evitarían los frentes de onda parásita

(principalmente ondas de superficie de Rayleigh) causados por reflexión artificial en los bordes del dominio computacional.

- Calibrar los modelos numéricos de los edificios usando técnicas de identificación de parámetros modales que incluyan la flexibilidad del suelo. Pese a que los modelos analíticos completos de base fija 3D brindan una buena referencia para la calibración del modelo 2D, un método experimental sería más acertado en la representatividad del caso de estudio.
- Caracterizar el sitio en profundidad. El modelo numérico muestra que el contraste de impedancia debido al estrato profundo de roca influye en el comportamiento no lineal de la superficie del talud; por ello, una opción adecuada es caracterizar el sitio en profundidad y extensión con mayor detalle usando métodos geofísicos basados en fuentes activas de gran energía o técnicas basadas en vibraciones ambientales con arreglos de gran tamaño.
- Incluir el comportamiento no lineal en las estructuras. Si bien los resultados mostraron que las edificaciones estudiadas tienen derivas de entrepiso pequeñas que hacen que se comporten principalmente dentro del rango elástico, otros registros de aceleración con diferentes amplitudes y contenidos de frecuencia podrían generar incursiones al rango inelástico de los edificios y de las estructuras de contención de tierras.
- Usar un modelo numérico completo 3D. Aunque dramáticamente demandante en términos de tiempo de cálculo computacional, reflejaría de mejor forma los efectos topográficos 3D, así como la tridimensionalidad de la señal de entrada

- Proponer y evaluar un procedimiento simplificado que considere el talud. Con fines de diseño estructural, un modelo analítico sencillo basado en osciladores y funciones de impedancia podría ser formulado, deducido y calibrado de manera que refleje patrones generales de la superficie en forma de talud.

El siguiente capítulo muestra el artículo enviado a la revista *Engineering Structures* que detalla el caso de estudio usado en este trabajo, así también como el procedimiento y resultados de esta investigación.

II. TOPOGRAPHICAL AND STRUCTURE-SOIL-STRUCTURE INTERACTION EFFECTS ON DYNAMIC BEHAVIOR OF SHEAR-WALL BUILDINGS ON COASTAL SCARP

II.1 Introduction

During seismic events, waves propagate from the source to site inducing dynamic loads to civil structures located near the surface. These structures interact with the surrounding soil, leading to interdependence of structural and soil domain responses. This dynamic soil-structure interaction (SSI) is rarely explicitly considered in seismic analysis and design of structures, but significant research has been carried out to introduce SSI effects on the design of single buildings located on horizontal soil surface (e.g. Choiniere, et al., 2019, Borbon et al., 2020). However, many times buildings are located on irregular topographies and close to other structures in urban areas, moving away from the usual hypotheses to include SSI. This is the case for example of many residential buildings located on coastal scarp, where the slopes are used to get clear views of the sea. The main purpose of this paper is to assess the influence of those features in seismic analysis of shear-wall buildings.

SSI have been an active research area for decades. More recently, structure-soil-structure dynamic interaction (SSSI), a subtopic that includes the additional interaction with near structures has been explored due to the densification of urban areas. These analysis provides an assessment of the modification of dynamic response related to the same buildings supported on rigid base. This response modification is mainly due to, (1) soil stratigraphy, (2) topographic effects, (3) energy dissipation by radiation from building's foundation toward deep soil strata, (4) inelastic behavior of soil, (5) pore

pressure build up, (6) inelastic structural behavior, (7) contact evolution at soil-structure interface, (8) dynamic cross-interaction effects with nearby structures and (9) intensity, duration and frequency content of input motion.

To analyze these complex phenomena, analytical and numerical solutions for static and dynamic SSI has been early proposed mainly for nuclear power and offshore industries as described by Kausel (2010), Menglin et al. (2011), and Roesset (2013). Substructure methods are the most rigorous for linear elastic systems. In this method, the problem is subdivided in various subdomains that are solved independently, kinematic and inertial interactions are included using transfer and impedance functions in frequency or time domain (Wolf, 1985, 1988). Unfortunately, these methods have many limitations in the consideration of complex soil geometries or heterogeneities and the impossibility of adequately represent nonlinearities. On the other hand, direct method using finite elements (Zienkiewics et al., 1999) is a good choice to conduct nonlinear dynamic analysis that can take into account complex geometries, the nonlinearities of porous media and foundations contact problem (gapping, sliding and uplift). Also, the radiation condition at the boundary of the soil domain can be approximated.

The effect of soil stratigraphy or "site effect" in the amplification of seismic motion has been studied for decades. More recently, the effects of soil topography in the modification of seismic motion gained interest. Assimaki et al. (2005) evidenced that topographical effects and diffraction of seismic wave due to soil stratigraphy and material heterogeneity can explain additively the high damage of a cliff crest and vertical response enhancement during 1999 Athens earthquake. Using parametric

linear elastic analysis, Zhang et al. (2018) shown the maximum acceleration amplification in a slope topography take place with a slope angle of 32° near the slope crest. Also Assimaki and Mohammdi (2018), Poursartip et al. (2017), Di Fiore (2010), Bouckovalas and Papadimitriou (2005), Nguyen and Gatmiri (2007), Paolucci (2002), Tadeu et al. (2001) emphasized the important role of irregular topographies in amplification and deamplification of seismic motion.

Limited studies exist regarding SSI including irregular surface topography. Alitalesh et al. (2018) studied a building located on top of an elastic slope, they obtained aggravation in vertical and horizontal acceleration by increasing the slope angle. Assimaki and Kausel (2007) studied the SSI of a simple building model with shallow foundation located behind the crest of a linear and nonlinear slope, they observed the filtering effect of high frequency in surface horizontal response, the generation of parasitic rocking motion at foundation level and the beneficial effect of SSI and foundation embedment on topographic amplification. On the other hand, previous studies of SSSI were limited to analytical and numerical results of simple models. Luco and Contesse (1973) and Wong and Trifunac (1975) identified key factors that determine the cross dynamic interaction between buildings such as distance between structures and the ratio of mass and stiffness between soil and structures. Using simple discrete models, Vicencio and Alexander (2018, 2019) reported that SSSI effects can increase responses of a small structure located near a tall structure. Alamo et al. (2015) studied the SSSI of nearby piled structures on horizontal soil surface and by means of linear dynamic analysis point out vertical incidence of input shear waves is not always the worst scenario, it suggests that slope topography and stratigraphy with vertical

seismic incidence can be a worst case. Also, more refined studies for particular cases are available. Han et al. (2020) realized 2D linear dynamic SSSI and they found that structural responses can reduce or increase up to 30% which depends on separation between buildings. Bolisetti and Whittaker (2020) conducted nonlinear 3D numerical analysis and they concluded that SSSI has negligible effect on the global spectral accelerations of low-rise buildings. These studies suggest that consideration of SSSI can be relevant in modification of seismic response.

Topographical effects are considered in a very simple way in few seismic design codes as Eurocode 8 (EC8). SSI has been supposed beneficial in majority of cases with no clear procedures to assess it, however some guidelines are provided in ASCE 7-16 (ASCE) and NTCS-17 (NTCS). Moreover, SSSI is usually disregarded in seismic design codes. However, there are reported cases in which SSI has played a detrimental role, intensifying damage of structures (Yashinsky, 1998; Mylonakis and Gazetas, 2000; Badry and Satyam, 2017) as well as SSSI effects increase building responses. From the literature review, topographical effects in buildings located near the crest of a slope combined with interaction effects with nearby structures and soil nonlinearity will modify in a complex way the seismic motion. It is not clear whether these effects will be beneficial or detrimental. Because the combination of these three effects is common in many recent residential projects on coastal scarp, the main goal of this study is numerically investigate the influence of topographical effects and SSSI effects in seismic analysis of medium-rise shear wall buildings located in a sandy hillside taking a reference real buildings as case study and considering non-linear dynamic structure-soil-structure interaction.

Firstly, a brief description of usual typologies of residential project on coastal scarp and details of the selected case study is presented. Secondly, vertical incident shear wave propagation is modeled to characterize the site and topographical effects on the site. Then, the structures are included in the models and 2D nonlinear time-domain dynamic analysis with vertical seismic input motion are made considering three cases: base fixed structures, SSI, and SSSI with slope topography to analyze the combined effect of topography and nearby structure on the seismic response of buildings. Finally, responses are summarized and discussed in terms of spectral ratios, forces and displacements indicators.

II.2 Case study

II.2.1 Description of site and buildings

Seaboard between Valparaíso and Reñaca located in the Valparaíso region in Chile is a high seismic hazard urban zone where low to medium-rise recent apartment buildings are typically placed in sandy hillside topography. Usually, the projects are made up of two independent buildings. The first, lower in height and located at the top of the hill, is used for parking lots. The second, where the departments are located, is taller and located on a lower level and faces the sea. Both buildings are connected by corridors or walkways. The hillside considered in this study has a mean slope angle of about 30° and approximately a height of 90m. The sandy soil in that zone is known as "dune sand" that consist of loose surficial sand and have an average thickness of about 5m. Below this depth, sand becomes dense with a variable degree of cementation in some cases usually referred as "old dune". The groundwater table is deep enough to neglect their effects. The first structure is a 28-story apartment building ("A") located

near the middle of a slope. The structural system is a typical Chilean reinforced concrete shear wall system referred to in the literature as "fish-bone" pattern (Westenenk, 2013) and the foundation is a 1.20m-thick slab supported over 8-10m length piles with a square section of 1m distributed below walls. The second structure is a small 8-story parking building ("P") located behind the "A" building, near the slope crest. It is also a reinforced concrete shear wall structural system supported by vertical and diagonal 10m length micropiles distributed along the perimetric and central wall foundations.

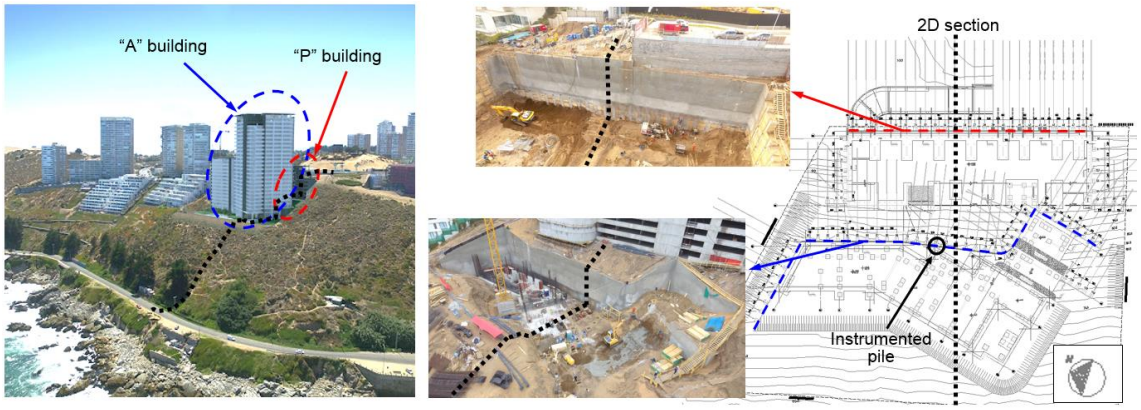

Figure II-1. General and Plan view of the case of study.

Prior to the buildings construction, the slope was lowered of about 16.5m and 17m for the "A" and "P" buildings, respectively. The earth retaining system were discontinuous reinforced concrete anchored pilling support systems with horizontal timber lagging covered by a double steel mesh and shotcrete. These square piles of 0.8m side length are separated each other 2.5m and they have between 2 and 6 anchor rows along their height. Both buildings are separated from earth retaining systems to avoid pounding.

Figure II-1 shows a global and plan view of the buildings and the slope, also the selected 2D section for the analysis described in the following

II.2.2 Soil characterization and static field measurements

A geotechnical investigation of the site was carried out including boreholes of 30-40m to perform SPT test and extract soil samples, also the shear wave velocity profile of the site was estimated based on surface wave techniques. Additionally, we perform laboratory test on samples from "dune sand" stratum to obtain strength parameters with triaxial test, and cyclic stiffness degradation and damping increasing curves using a combined cyclic torsion and resonant column device.

One of the anchored piles located between both buildings were instrumented with an inclinometer (Figure II-1b) and lateral deflection measures along construction process were made. Raddatz and Taiba (2018) present the pile lateral deflection for six stages that corresponds to final state of excavations and post-tensioning of steel tendons. Also, they present force-deformation curves for two micropiles of "P" building which were tested by a tensile extraction load test. This information was used in the calibration process of the material parameters and to perform static verification of the numerical model as described in the following section.

II.3 Numerical modelling

II.3.1 FE model and calibration

Due to the high computational cost of dynamic nonlinear analysis of 3D structures using the direct method, an equivalent 2D plain-strain finite element model of the soil-structures system were constructed using Plaxis2D software (Plaxis2D, 2020). First,

full 3D modal analysis of detailed models “A” and “P” buildings were done to obtain their frequencies and modal shapes. Then, a representative frame of the buildings in the direction of the slope were selected and 2D simplified models were calibrated such that they were able to represent the 3D buildings in terms of seismic mass, frequencies of vibration and modal shapes.

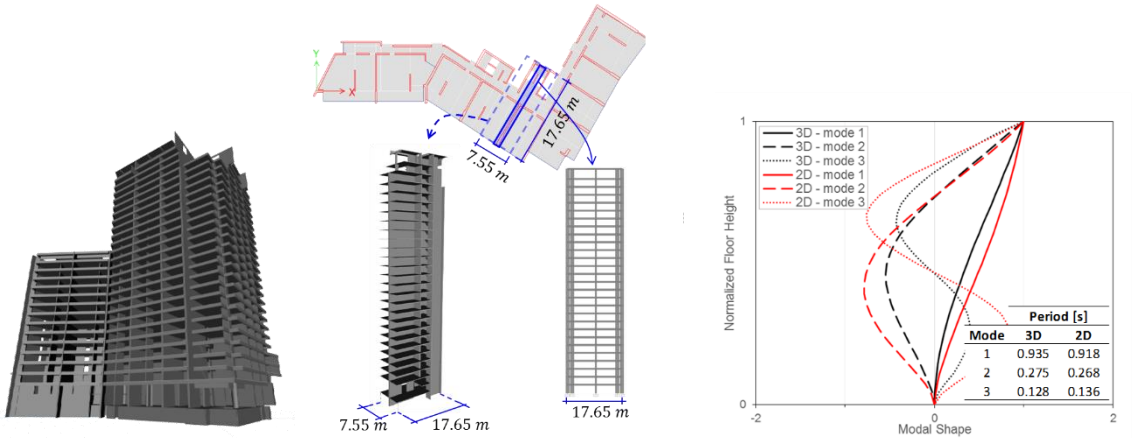

(a)

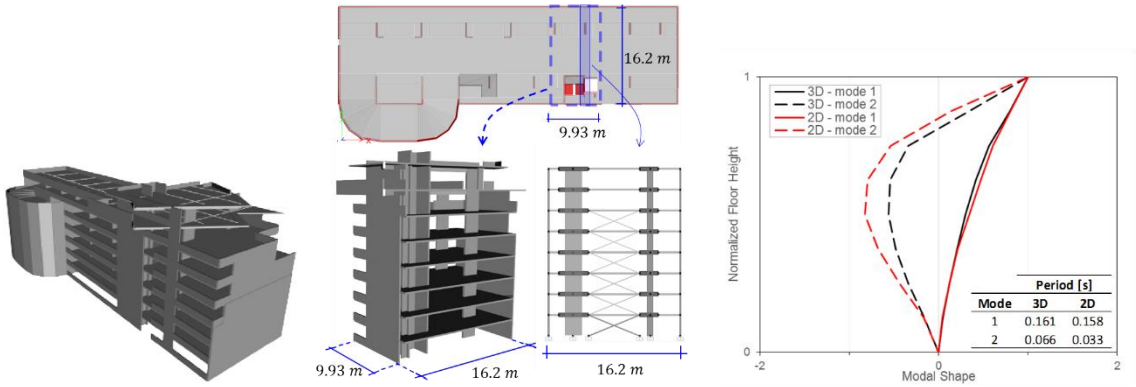

(b)

Figure II-2. Left panel: 3D view of the numerical model of buildings. Central panel: plan view, representative 3D frame, and elevation for 2D model. Right panel: Modal shapes and Periods of full 3D and adjusted 2D building model (a) “A” building, (b) “P” building.

The hardening soil model with small-strain stiffness (Benz, 2007) (HS small) was used to model the cyclic elastoplastic soil behavior because takes into account the confinement dependence of soil stiffness and the energy dissipation at very small strains. The experimental and simulated paths for drained triaxial tests at 70, 140 and 280 kPa of initial confinement, as well as shear modulus degradation and damping curves at 50 kPa are shown in Figure II-3. The HS small shows a reasonable agreement against experimental results, but the model is unable to reproduce post peak softening. Nevertheless, the maximum expected seismic deformations are of about 0.3%, i.e. the adjustment at low deformation is the most relevant.

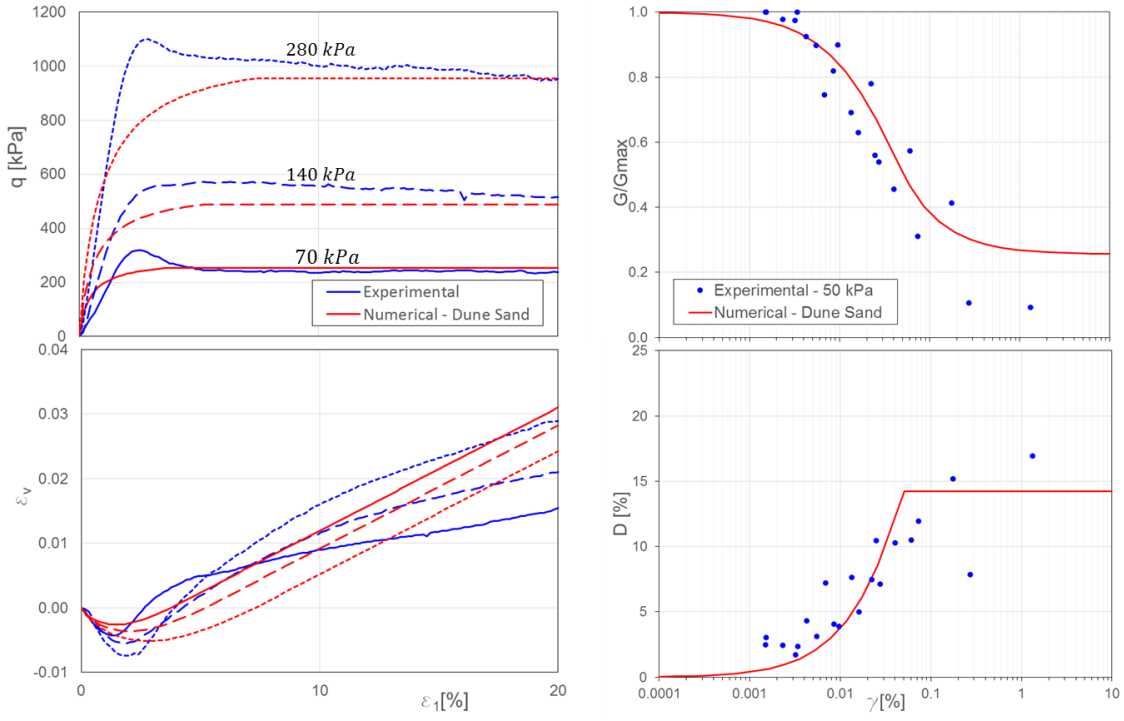

Figure II-3. Experimental and numerical curves. Left Panel: Triaxial CID of "dune sand". Right Panel: Shear modulus degradation and damping curves.

The discontinuous piles and anchor's grouting, foundation piles and micropiles were modeled using the embedded beam row element (Sluis et al., 2013). The anchor free length was modeled by node-to-node elements, where the prestress was applied according to excavation stages. Because inelastic soil behavior is triggered at very small deformations, the structural elements were assumed to behave elastically. Nonlinear interfaces based on Mohr-Coulomb sliding criterion were considered at the structure-soil contact allowing opening. Free-field boundaries were used at lateral boundaries of the model to absorb outgoing waves. Moreover, a zone of 50m-width with additional material damping were added near the lateral boundaries of the model to improve the absorption of generated Rayleigh waves. The finite element mesh was generated using 15-node triangular element to ensure at least twelve nodes in the shorter wavelength related to the maximum frequency of the input signal. A general view of the model is shown in Figure II-4.

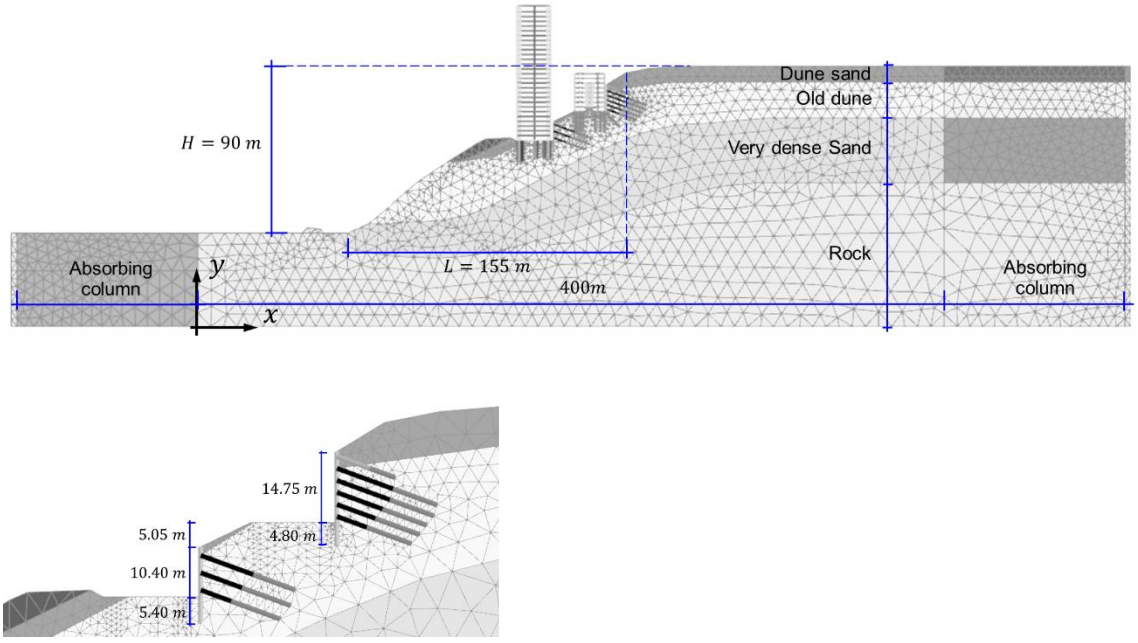

Figure II-4. General and local view of the finite element model.

The excavation, construction of piles, prestressing of anchors and sequential construction of buildings were considered in the numerical modelling. As validation of the FEM model, the measured lateral deflection of the instrumented pile is compared against numerical results in Figure II-5a. Also, the experimental shear wave velocity profile is used to verify low-strain soil stiffness in the FEM model (Figure II-5b). The inclinometer data was corrected for rotation error (Mikkelsen, 2003), after that, it's observed the deflection of the pile are well approximated for the stages in the upper part of the pile, but the measures in the middle part tell the soil-pile is more flexible for stages 3 and 4. These differences might be related to the 2D embedded pile model that approximates a "mean" 3D soil effect, and additionally, to the instrument used since they are quite small deformations in the limit of the precision of the equipment. In general terms, a reasonable agreement was found between numerical and measured deflections of pile.

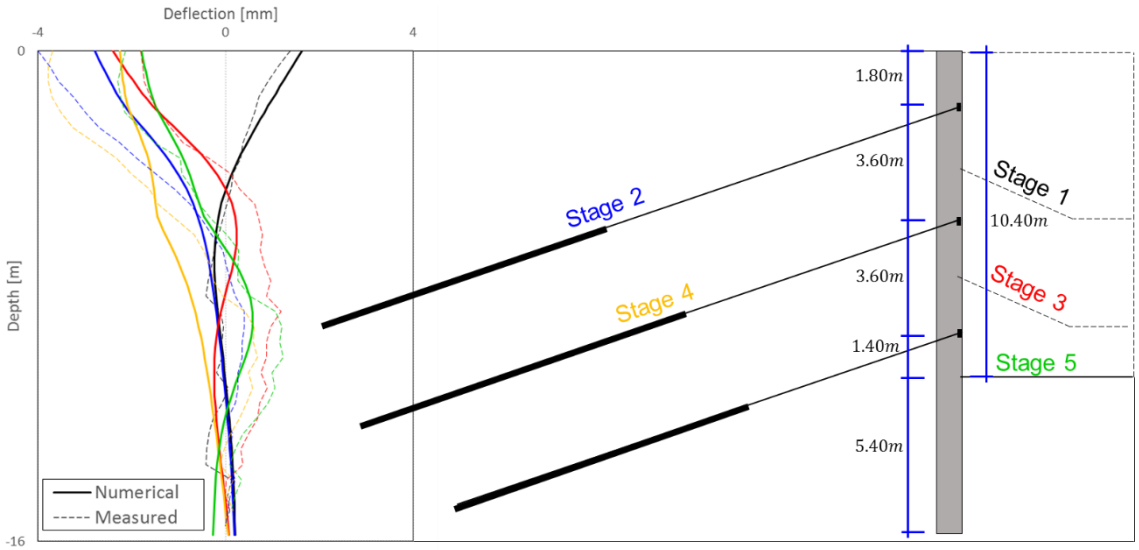

(a)

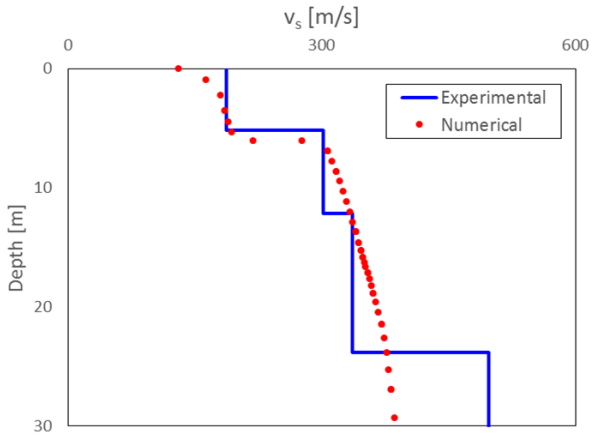

(b)

Figure II-5. (a) Deflection of instrumented pile in mm. (b) Vs profile. General and local view of the finite element model

Classical Rayleigh damping of 5% was considered for both buildings while 3% was used for the soil. Since the constitutive model of the soil generates energy dissipation by hysteresis, the purpose is to provide a minimum damping in the range of small deformations when the soil model is in the elastic range. The material parameters of the soils and structural model are summarized in Table II-1 and Table II-2.

Table II-1. Parameters of soil for linear material model.

Parameter	"Dune sand"	"Old dune"	Very dense sand	Rock	Unit
E	290	433	760	3000	MN/m²
ν	0.25	0.25	0.25	0.30	-
γ	17.5	18.0	19.0	22.0	kN/m³

Table II-2. Parameters of soil for HS small material model.

Parameter	"Dune sand"	"Old dune"	Very dense sand	Unit

E_{50}^{ref}	39570	78620	116400	kN/m²
E_{oed}^{ref}	39570	70000	93080	kN/m²
E_{ur}^{ref}	80000	160000	349100	kN/m²
m	0.5	0.5	0.5	-
c'	4.91	4.91	4.91	kN/m²
ϕ'	39	41	46	°
ψ	5	0	0	°
$\gamma_{0.7}$	0.00263	0.00200	0.00145	-
G_0^{ref}	125830	250000	370000	kN/m²
v_{ur}	0.25	0.25	0.25	-
p_{ref}	100	100	100	kN/m²
K_0^{nc}	0.3707	0.3439	0.2807	-

II.3.2 Topographical effects

Prior to analyze the full interaction problem, topographical effects were studied in the unexcavated slope topography to assess its amplification and deamplification potential. Perfectly vertical incidence shear wave propagation of Ricker pulses with different central frequencies of 0.8, 1.5, 2.5 and 5 Hz were used to cover a frequency range between 0.5 and 10 Hz where buildings, site and seismic motion are content. There are many definitions of topographical amplification ratios or topographical aggravation factors (e.g. Apostolos et al., 1991; Assimaki et al., 2005) generally in terms of 2D/far-field acceleration spectral ratios. Here, a similar definition than Zhang et al., (2018) were used due to overcome the problem of constant far-field reference points that is not available for target problem. In this study, the topographical amplification factor (TAF) and vertical aggravation factor (VAF) were defined over the surface of the soil domain as follows.

$$TAF(x,f) = \frac{|\mathcal{F}\{\ddot{u}_x(x,t)\}|_{2D}}{|\mathcal{F}\{\ddot{u}_x(x,t)\}|_{1D}} \quad (2.1)$$

$$VAF(x,f) = \frac{|\mathcal{F}\{\ddot{u}_z(x,t)\}|_{2D}}{|\mathcal{F}\{\ddot{u}_x(x,t)\}|_{1D}} \tag{2.2}$$

Where x is the horizontal coordinate, f the frequency, $\ddot{u}_x\ (x,t)$ and $\ddot{u}_z\ (x,t)$ are the horizontal and vertical acceleration at surface, respectively $|\mathcal{F}\{\cdot\}|$ stands for the modulus of Fourier amplitude of the time-dependent variable, and the subscripts 2D and 1D indicate the numerical model used to compute the value. 1D values were obtained from a 1D-column with the same material and layer depths, using the same input motion of the 2D model. This 1D reference is used to quantify the one-dimensional soil column motion modification effect. The TAF and VAF definitions are illustrated in Figure II-6.

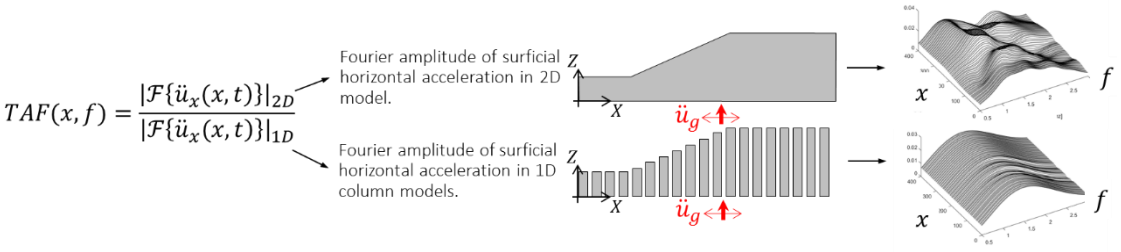

Figure II-6. Graphical representation of the Topographical Amplification Factor (TAF).

First, linear cases were studied to have an insight in the wave propagation phenomena. Then, nonlinear soil behavior was included, and excavated soil profile without buildings was taken into account. In nonlinear models, the amplitude of the ground motion matters, for this reason, two maximum amplitudes of Ricker pulses in the surface of a bedrock were used: 0.1 and 0.4g to include low and moderate soil inelastic behavior. Also, seismic records were used as shown in section II.3.4.

II.3.3 SSI and SSSI effects

Buildings were modeled in three scenarios. First, reference case of fixed-base (FB). Then, to evaluate the influence of interactions, two additional cases were considered: soil flexibility effects on individual buildings (SSI) where only the excavation and retaining wall of the foundation of the adjacent building are considered, and the dynamic cross-interaction effect between soil and both buildings (SSSI). The considered ground motions are described in section II.3.4.

Two spectral ratios were proposed to have an insight of SSI and SSSI $|H_{\ddot{U}_x}|$ and $\left|H_{AX/Z}\right|$, the former shows the structural behavior of buildings while the latter show a wide panorama of soil-structure interaction. The *j*-th floor components of the first ratio is:

$$H_{\ddot{U}_{xj}} = \frac{|\mathcal{F}\{\ddot{u}_{gx} + \ddot{u}_{x0} + \ddot{\theta}h_j + \ddot{u}_{xj}\}|}{|\mathcal{F}\{\ddot{u}_{gx} + \ddot{u}_{x0}\}|}\Bigg|_{FB,\ SSI,\ SSSI} \tag{2.3}$$

Where the variables are shown graphically in Figure II-7, $|\mathcal{F}\{\cdot\}|$ stands for the modulus of Fourier amplitude of accelerations, u_{gx} is the ground motion, u_{x0} is the relative horizontal deformation between the rigid body motion of the foundation, θ is the rotation of the foundation as rigid body, h_j is the height to the floor j and u_{xj} correspond to the relative horizontal displacement. The subscripts FB, SSI and SSSI stands for the considered case.

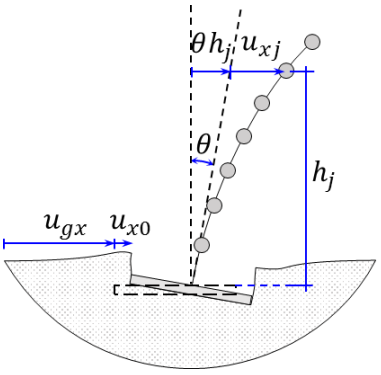

Figure II-7. Idealized variables.

The second ratio for accelerations is:

$$H_{AX} = \frac{|\mathcal{F}\{\ddot{u}_x\}|_a}{|\mathcal{F}\{\ddot{u}_x\}|_b}, H_{AZ} = \frac{|\mathcal{F}\{\ddot{u}_z\}|_a}{|\mathcal{F}\{\ddot{u}_z\}|_b} \quad (2.4)$$

Where $\ddot{u}_x$ and $\ddot{u}_z$ are the horizontal and vertical absolute acceleration in the soil surface, and a and b stand for one of the follow three cases: (a) non-excavated slope profile, (b) excavated slope profile without buildings and (c) excavated profile with both buildings

II.3.4 Ground motion selection

To perform a comprehensive evaluation of the SSSI and topographic effects, four Ricker wavelets were used with different central frequencies (f_0) that covers the frequencies of interest where interaction could appears. Their amplitude was adjusted to trigger different levels of inelastic soil behavior. In addition, two far-field earthquake ground motion records from instruments located in rock were selected for dynamic nonlinear analysis. These records correspond to the Algarrobo and the Maule earthquakes with epicenters in the region of Valparaíso and Maule, respectively, in

central Chile. Some significant characteristics of these records are listed in Table II-3, and their frequency Fourier spectrum is shown in Figure II-8.

Table II-3. Earthquake ground motions used and their principal features.

Earthquake record	Station	PGA (g)	Mw	Arias intensity (m/s)	Significant Duration (s)	Mean Frequency (Rathje et al., 1998) (Hz)
Algarrobo 1985 – comp. 70	UTFSM	0.17	8.0	1.12	38.96	4.6
The Maule 2010 – comp. NS	RAPEL	0.21	8.8	2.05	34.27	2.4

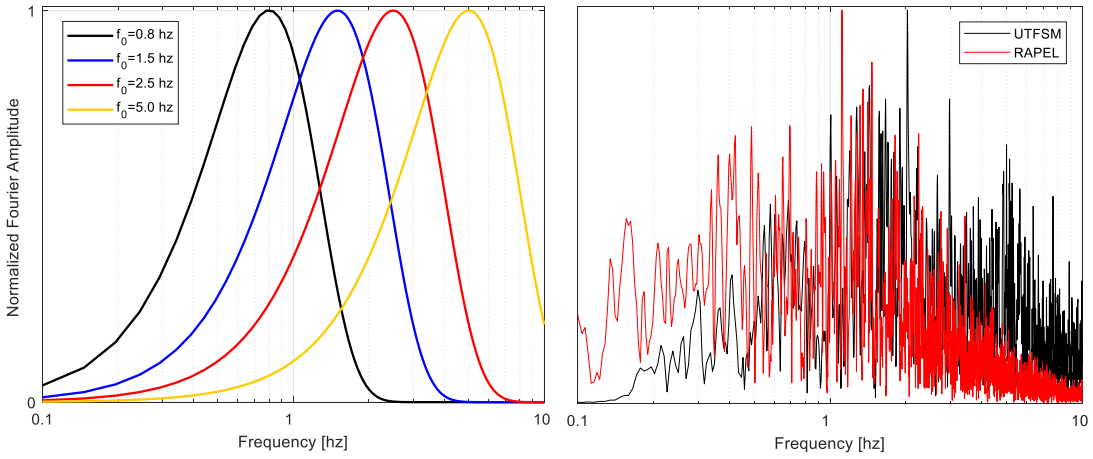

Figure II- 8. Normalized Spectrum of Fourier Amplitude for: Left Panel. Ricker pulses. Right Panel. Seismic records

II.4 Results and discussion

II.4.1 Topographical effects

To assess pure topographical effects and to provide a reference to heterogeneous and nonlinear cases, a simplified version of the actual slope with homogeneous linear

material corresponding to the "dune sand" strata are analyzed. Vertically incident shear planewave Ricker pulse (horizontal particle motion) with central frequency of $f_0 = 5\ Hz$ is used. Figure II-9 shows the propagation of acceleration waves along the surface of the slope, those waves are: the direct SV wavefront (SV), the Rayleigh waves (RW) generated in the toe and in the crest of the slope because the slope angle exceeds a critical angle (Semblat and Pecker, 2009; Zhang, et al., 2018), and P-waves (P) generated as a reflection of the incident wavefront along the slope. These waves propagate to the left (L) and to the right (R) direction along the model surface. Note that surface waves interfere constructively with direct SV near the crest of the slope. Also, a vertical component of motion appears in the surface response due to the diffraction of vertical input waves along the surface of the slope and retrograde motion of Rayleigh waves, i.e., topographical effects.

Although the frequency content of the generated waves (around f_0) remain almost the same, its amplitude varies with the position along the model because constructive and destructive wave interference takes place. Figure II-10a shows that behind the crest exists a zone where the maximum horizontal amplitude occurs followed by a narrow zone where amplitude drastically decreases. This pattern is repeated over the model surface at distances that are dependent of the ratio between the characteristic wavelength of the incident motion (λ_0), it is $\lambda_0 = V_s/f_0 = 62\ m$, and the height of the slope $H = 90\ m$. It means that the surface response is input frequency dependent as it can be noted from the same figure for the Ricker pulse with a central frequency of $f_0 = 2.5\ Hz$ where this pattern is stretched. Additionally, maximum Fourier amplitudes of vertical surface acceleration response are close to one third of the

horizontal ones and their peak values are not necessarily located at same place. These results reveal the complex wave propagation pattern that occurs in this simple topographic feature.

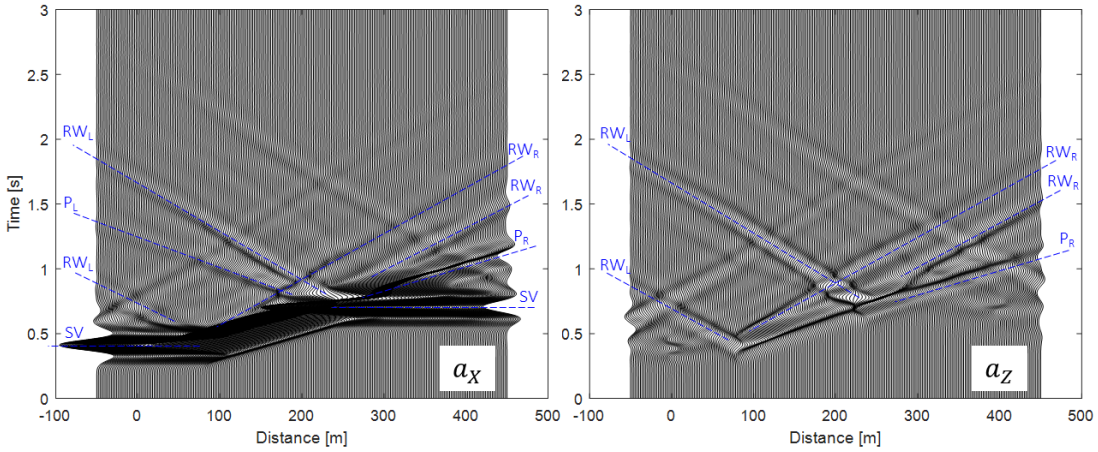

Figure II-9. Seismogram of horizontal and vertical acceleration surface response for a Ricker pulse with central frequency of $f_0 = 5\ Hz$.

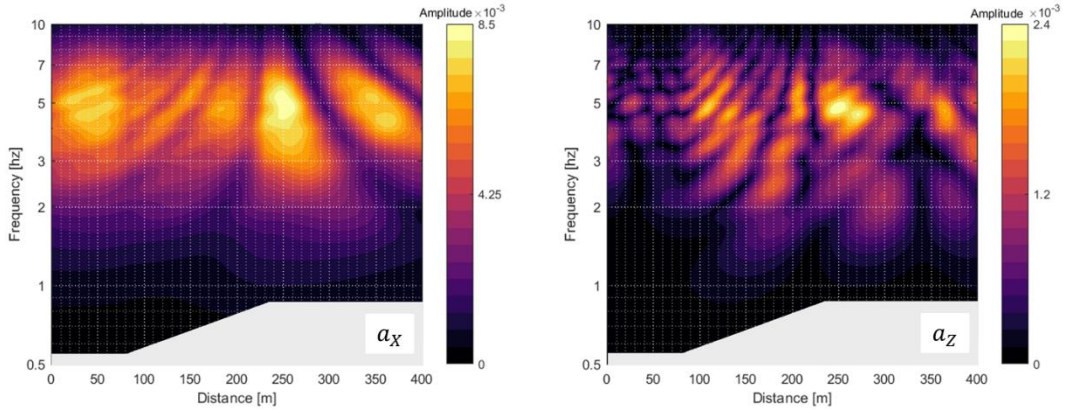

(a)

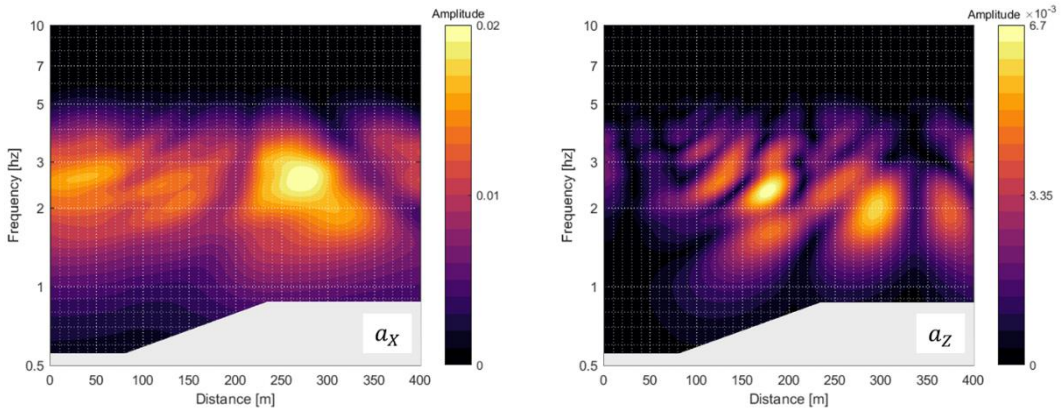

(b)

Figure II-10. Fourier amplitude of horizontal and vertical acceleration on the surface of the model for two Ricker input pulse with central frequencies of (a) $f_0 = 5\ Hz$. (b) $f_0 = 2.5\ Hz$.

In view of the previous results, four models with linear material models where studied: i) a gentle slope (slope angle of 15°) with homogeneous material, ii) simplified slope (slope angle of 30°) with homogeneous material, iii) slope with actual topography but homogeneous material, and iv) slope with actual topography and all soil strata. The expressions shown in Equation 2.1 and Equation 2.2 were used to build Figure II-11 in the frequency range of interest.

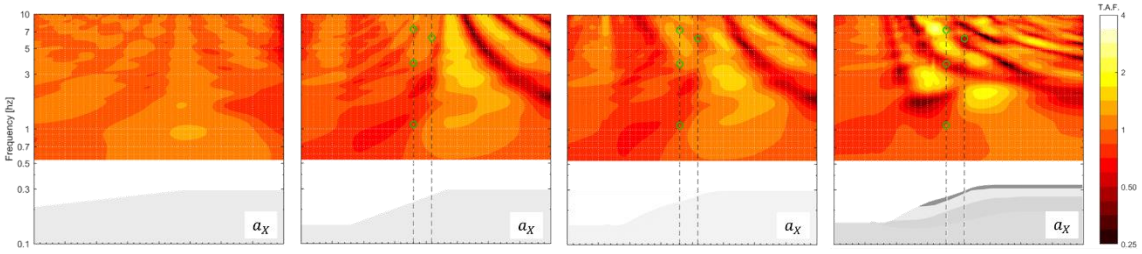

(a)

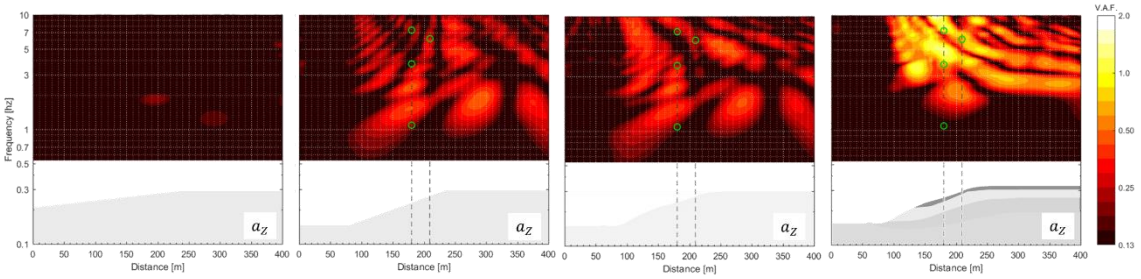

(b)

Figure II-11. Left panel: Gentle slope. Central left panel: Simplified slope. Central right panel: True topography with homogeneous material. Right panel: True topography and heterogenous soil strata. (a) Topographical amplification factor (TAF), (b) Vertical aggravation factor (VAF). The dashed lines indicate the location of buildings with their fixed-base natural frequencies of vibration (green circles).

The gentle slope shows limited values of TAF in the distance-frequency domain. Indeed, a maximum value of 1.3 is located just in the crest for $f = 2.2\ Hz$, suggesting that slope is not steep enough to trigger significant diffraction of input SV waves. For the second case, the tendency is clear and the maximum value of TAF are located not necessarily at the crest of the slope but behind it due to phase difference and superposition of P waves and Rayleigh waves that appear due to the slope angle. In this location ($x \approx 260\ m$), the TAF begins to be appreciable with a maximum value around 2 for $f \geq 3.4\ Hz$. This frequency range corresponds to the solution for f for the inequation $\frac{\lambda_0}{H} \leq 1$, (see Figure II-4), i.e. the characteristic wavelength of input motion are comparable or lower that the characteristic height of the slope and they interact. Also, it can be noted that for low frequencies $f < 1$ Hz, no 1D amplification

occurs at this location, and the same is valid for the zone between the toe and the crest of the slope where the effects of wave interference are small.

For the second case, the VAF, just like the TAF, appears in a characteristic frequency range related to the ratio $\frac{\lambda_0}{L} \leq 1$ (see Figure II-4). Hence, for $f \geq 2\,Hz$ the VAF becomes considerable with maximum values of about one-half of the horizontal component, and these values are located not only to the right of the crest of the slope but also to the left. This suggests that for geometric ratios of the slope $H/L < 1$, the VAF becomes important from frequencies lower than the TAF. Namely, vertical aggravation takes effects on a broad frequency range and location than horizontal aggravation but its magnitude is less important. This is due to purely topographic effects and the specific slope angle.

The third case shows that despite the fact the maximum values of TAF and VAF remain very similar than previous case, small changes in the surficial topography profile can significantly shifts the location and maximum values. The round corners of the toe and crest of the slope make TAF decrease at these locations, while the VAF tends to be concentrated in the concave surface at $x \approx 120\,m$ for high frequency values where wavelengths can interact with this ground feature. The four case shows that the stratified soil introduce additional complexity in the wave propagation, it enhances TAF's maximum values in localized zones where the surficial layer is the loose "dune sand", specifically at $x = 150\,m$ and $f = 3\,Hz$ and in the vicinity of the crest in which upward waves are trapped by the multiple reflections and refractions through impedance contrast that shift their direction of propagation to the left. Also, VAF is substantially enhanced.

Of course, even for moderate earthquakes, the soil behaves in a nonlinear way and usually their properties depend on the depth. For this reason, the inelastic behavior of soil was considered in left and central left panel of Figure II-12, in which the results for four Ricker pulses of different central frequencies were combined to have a continuous plot up to 7 Hz. As expected, nonlinearity gives a better estimate of TAF and VAF with reduced values of maximum aggravation factors. It is interesting to note that as amplitude of input increases, TAF decreases and VAF increases. The former can be explained because larger motions increase yielding and energy dissipation in surficial layers. Indeed, these layers acts as a band pass filter for high frequency accelerations. Moreover, the soil experiences non-linear behavior mainly driven by shear, with a coupling with dilatation that is relatively limited in the range of shear deformations explored (up to 0.3%), therefore it is the horizontal component that is more attenuated.

Although those phenomena are not directly related to the topographic effects, the general pattern of TAF and VAF remain very similar to those of linear cases but enhanced by site characteristics. The same is true when seismic records are used as shown in the right and central right panel of Figure II-12 where the wide frequency content of seismic records blur the plots. However, the maximum values of TAF and VAF also remain around 2 and 1, respectively. It is interesting to note that Eurocode 8 (EC8) suggest a topographical factor ≥ 1.4 that decrease linearly from the crest to the base of the slope, being the unity at the base. According to our results, this very simple frequency-independent factor can be unconservative for a maximum of about 43% for some frequencies and locations along the slope of this case of study.

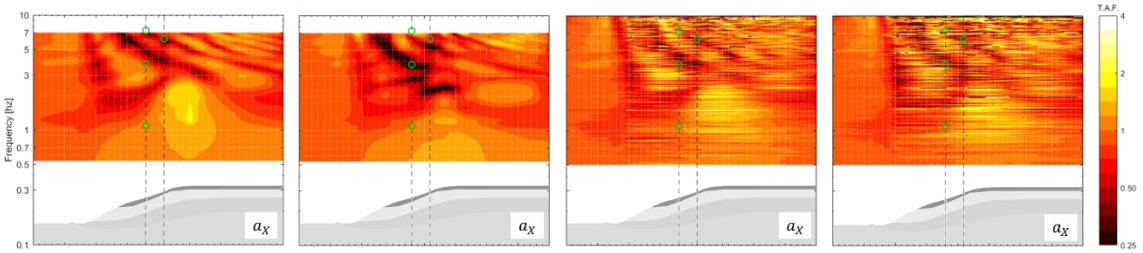

(a)

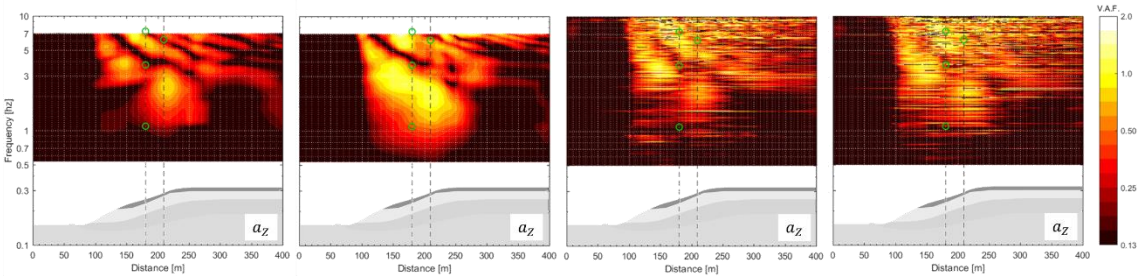

(b)

Figure II-12. Nonlinear stratified soil with two different inputs. Left panel: Ricker pulses with PGA of 0.10g at outcropping bedrock. Central left panel: Ricker pulses with PGA of 0.40g at outcropping bedrock. Central right panel: UTFSM seismic record. Right panel: RAPEL seismic record. (a) Topographical amplification factor (TAF), (b) Vertical aggravation factor (VAF). The centerline of buildings where they will be located are shown in dash lines with their fixed-base natural frequencies of vibration.

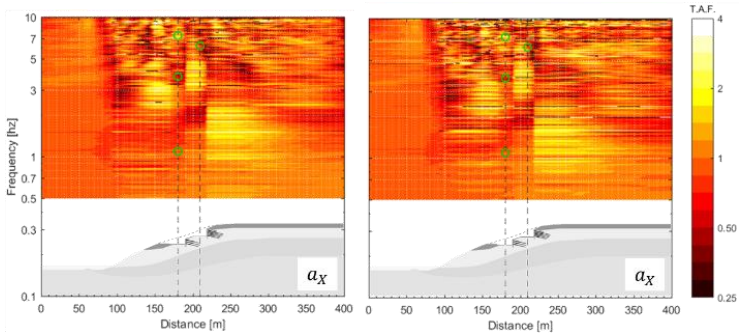

(a)

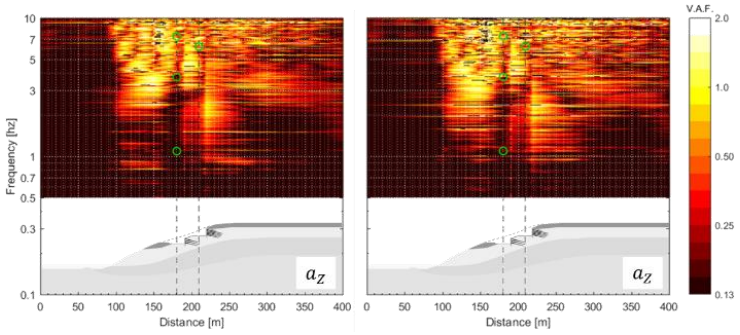

(b)

Figure II-13. Nonlinear stratified soil with excavation and inputs: Left panel: UTFSM seismic record. Right panel: RAPEL seismic record. (a) Topographical amplification factor (TAF), (b) Vertical aggravation factor (VAF). Dashed lines mark locations of buildings and green circles indicate their fixed-base natural frequencies of vibration.

Finally, to have and insight about the excavated topographical profile, excavation and earth retaining where included in the simulation. Figure II-13 shows that TAF increase at $f = 4.3\ Hz$ behind the left retaining wall system, this is the frequency associated with the approximated first mode of vibration of this wall ($\frac{v_s}{4h_w} = \frac{\sqrt{0.65}*307m/s}{4(14.5\ m)} = 4.3\ Hz$) where modulus degradation of 65% were approximated for the soil mass in accordance with results and Figure II-3 for a mean shear deformation of 0.03%. Also, these trapped waves interact with this left wall in the vertical direction, increasing VAF at the same frequency. On the contrary, for low frequencies (<4 Hz), the low confinement of soil below excavation grade decrease values of TAF and VAF (soil have minor acceleration compared to 1D case). In summary, sharp topographies can

completely shift topographical amplification for certain resonant frequencies and particular zones. In this specific case, tall buildings of low natural frequencies could be little affected, while low-rise buildings of high natural frequencies could experience amplifications.

II.4.2 SSI and SSSI effects

Main results of the three scenarios described in section II.3.3, four Ricker input pulses scaled at two amplitudes and two seismic records are shown in Figure II-14. The maximum interstory drift, corrected by rigid body rotation of building, are below 0.002 for all cases in Figure II-14a, i.e. similar buildings of this typology remain in the smooth ascending zone of pushover curves (Ugalde et al., 2019) with an approximate elastic behavior. In general, the structural responses are incremented when central frequency of the input are near the fundamental frequencies of vibration of the buildings (1.1 Hz for "A" building and 6.3 Hz for "P" building) as a resonance-like effect, but topography and soil introduce additional effects as is discussed in the following.

In general terms, i) a significant increase of vertical acceleration can be noted for both buildings because of the topographical effects. In all cases, these values are below 2/3 of horizontal acceleration as shown in Figure II-15d, criterion commonly adopted for design of buildings on horizontal sites. ii) SSI and SSSI scenarios have beneficial effects regarding the reduction of structural responses of "A" building for all input cases. This happens because this building is very flexible compared with characteristic frequencies where topographical effects appears, i.e. the structure is far from topographical effects zone, even though this structure has significant modal mass ratio

of second and third vibration modes (about 13% and 5% respectively). Furthermore, due to SSI effects, radiation damping and hysteretic soil damping, there are additional energy dissipation in comparison to FB scenario. From a design point of view, this SSI effect can be interpreted as a period lengthening of the structure (inertial effects) reducing the spectral pseudo-acceleration ordinates. This is shown in Figure II-16a and 16b for "A" building. iii) However, SSI and SSSI scenarios have detrimental effects for "P" building at low frequency, this is also shown in the reduction of responses in Figure II-15a, Figure II-15b and Figure II-15c where points of "P" building have negative reduction of responses (increase of responses) relative to fixed-base scenario, up to 80% for interstory drift and 35% for seismic coefficient. Also Figure II-16a shows this effect because the lengthening of the fundamental period increases the spectral ordinates. However, for the characteristic far-field seismic inputs in Figure II-15c, this effect is much less important due to the wide frequency content of the record in the zone of high frequencies (lower periods) and it is beneficial in other several cases. iv) In some cases, SSSI scenario enhance the beneficial and detrimental structural responses. This is observed in Figure II-14d where majority of points with positive reduction are above the 1:1 line and points with negative reduction are under the diagonal line. This is probably because the vibrations of the second structure interfere constructively or destructively (depending on the frequency) with the vibrations of the neighbor structure. This cross-interaction effect happens between the soil located at piles' level of "A" building and micropiles' level of "P" building, and their effect causes local modification of motion that slightly attract and reject energy and induce the enhancement of structural responses. This interaction is also affected

by the anchored wall system between buildings. Indeed, this structure probably interferes a direct propagation of waves between buildings, especially for short wavelength waves.

In addition, the seismic effect is shown in Figure II-14 and Figure II-15. These cases behave approximately in a similar manner of cases with Ricker input with central frequency of 2.5 Hz and amplitude of 0.40g mainly because this is approximately the central frequency of the UTFSM and RAPEL seismic records.

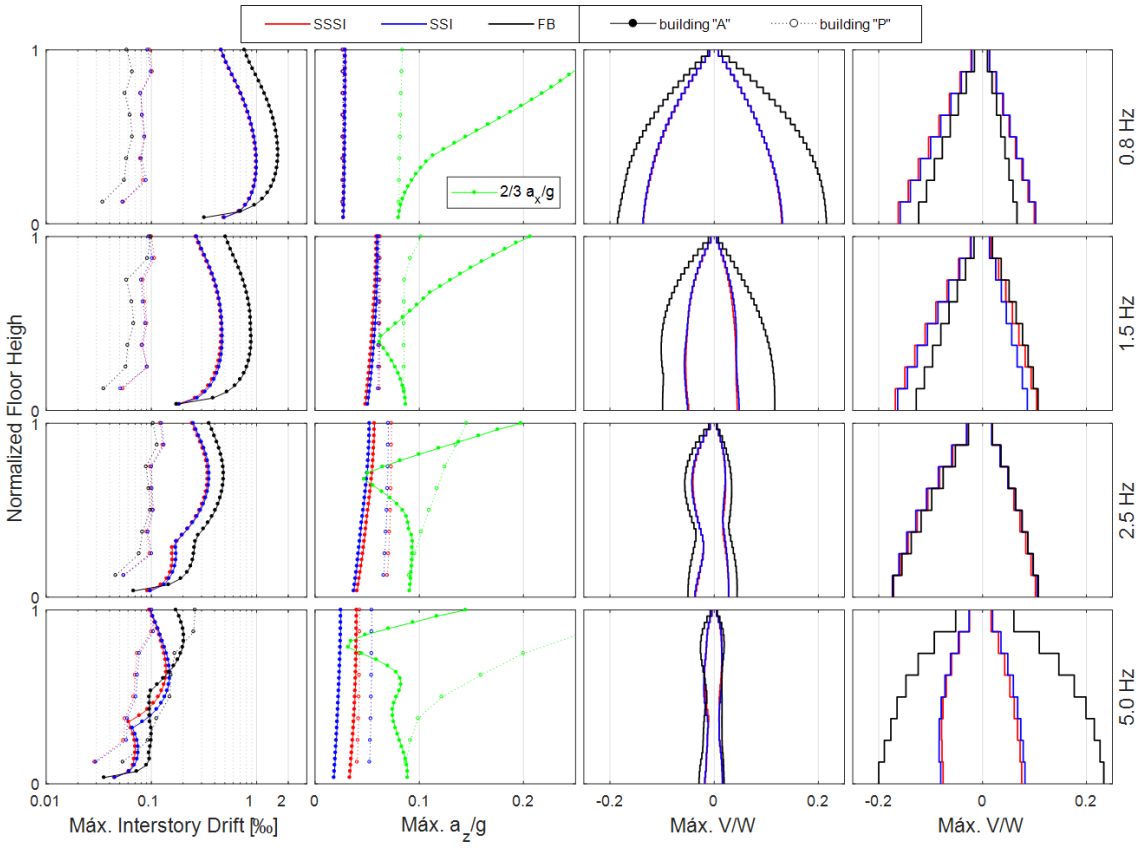

(a)

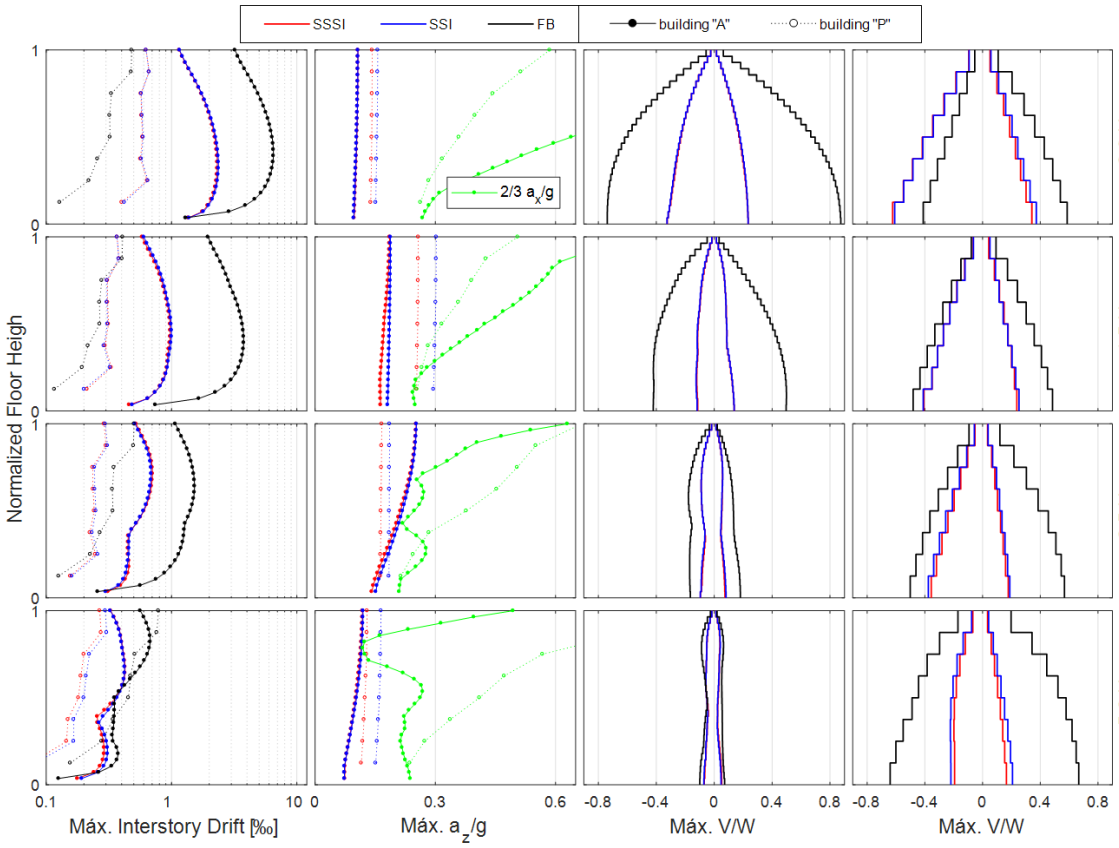

(b)

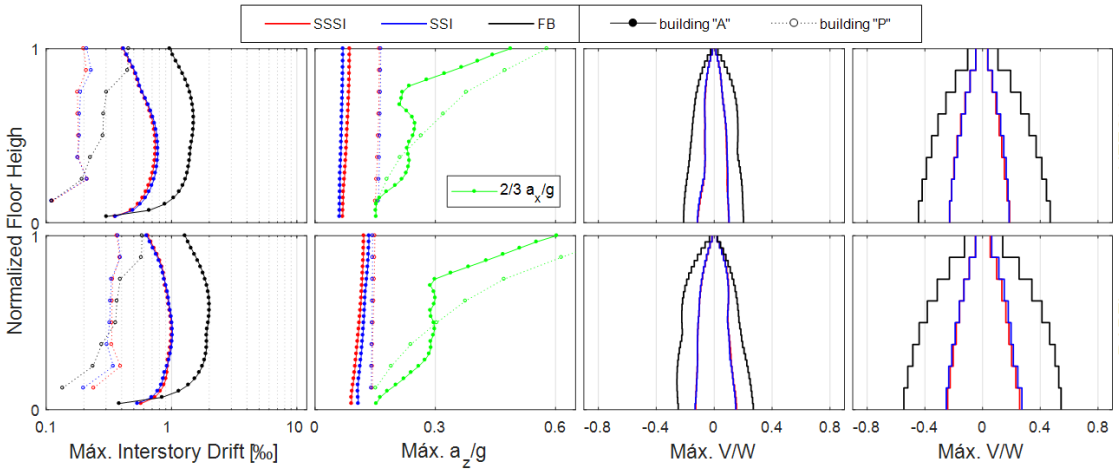

(c)

Figure II-14. Structural responses of max. interstory drift, max. normalized absolute vertical acceleration, and max. seismic coefficient (normalized shear force) in

buildings “A” and “P” for three scenarios (FB, SSI and FB) and Ricker input pulses with central frequencies of 0.8, 1.5, 2.5 and 5.0 Hz and seismic records (a) Ricker with PGA of 0.10g at outcropping bedrock. (b) Ricker with PGA of 0.40g at outcropping bedrock. (c) UTFSM and RAPEL records.

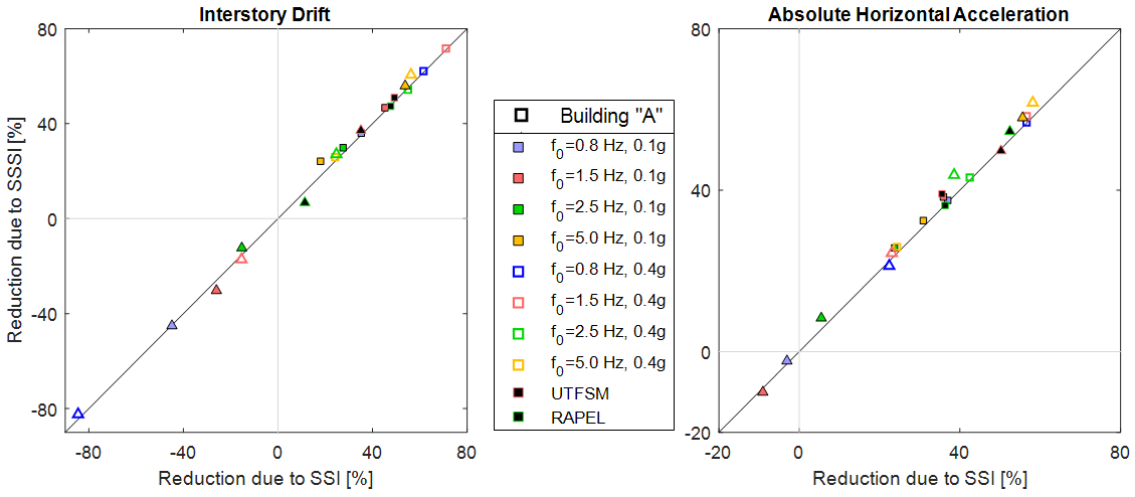

(a) (b)

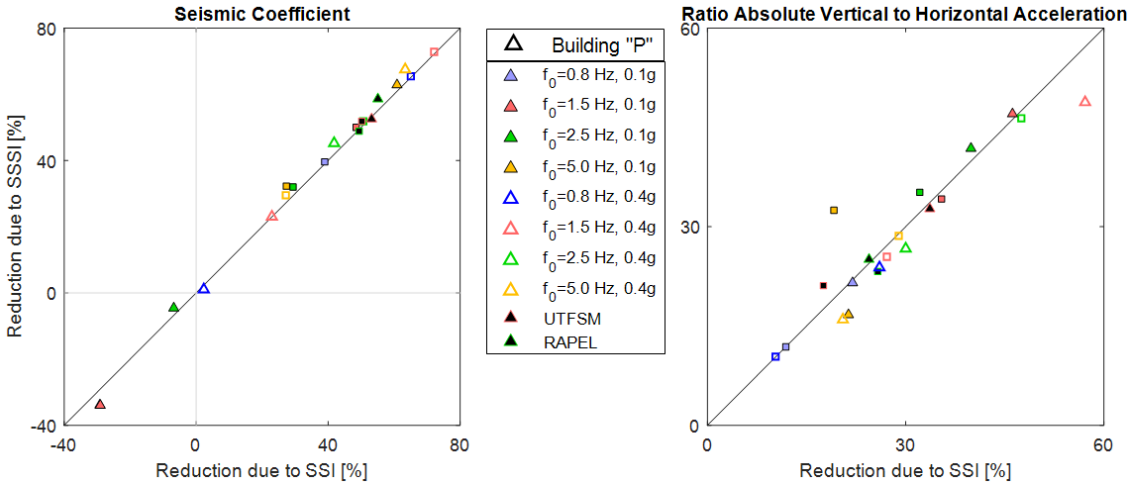

(c) (d)

Figure II-15. Reduction of structural responses due to SSI and SSSI regarding FB scenario. (a) Interstory drift. (b) Absolute horizontal acceleration. (c) Seismic coefficient (normalized shear force), and (d) Absolute vertical acceleration with respect to horizontal one.

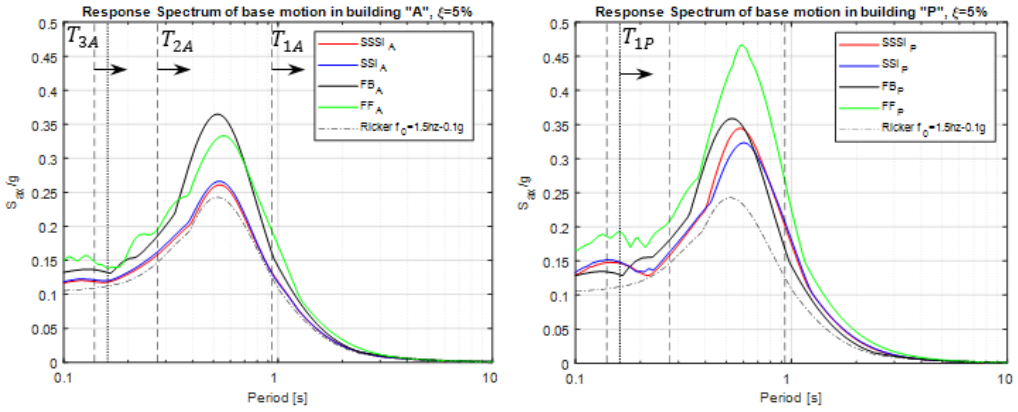

(a)

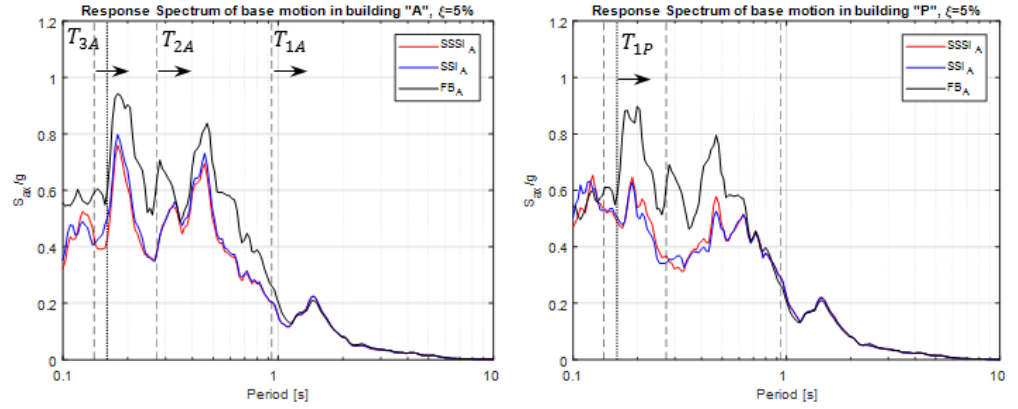

(b)

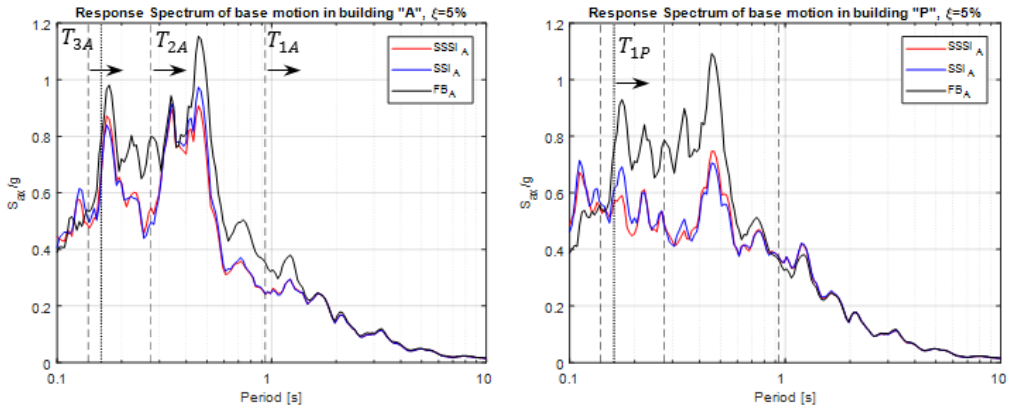

(c)

Figure II-16. Spectrum of horizontal pseudo-acceleration at base of buildings for three scenarios: (a) Ricker 1.5 Hz - 0.10g. (b) UTFSM. (c) RAPEL. Fixed-base vibration periods of both "A" and "P" buildings are shown in dashed and dotted lines, respectively.

Spectral ratios described in section II.3.3 are shown in Figure II-17. The lengthening of periods of vibration of both buildings are clearly observed for the SSI scenario, while SSSI scenario has negligible additional effects. This lengthening is as expected for "A" building as indicated in Table II-4. However, it is large than anticipated for the "P" building. In this last case the excavation induces peak values of TAF and VAF at about $f = 4\,Hz$ behind the retaining wall, i.e. near the fundamental frequency of the "P" building and probably these trapped waves interact with the building as an added mass effect. Also, the kinematic of "P" building is affected by a rocking due to soil-structure system coupling. Moreover, local soil yielding on the sides of foundation induced by this rocking motion enhanced this interaction as can be shown in Figure II-19 where the strain-hardening parameter of the soil (γ^p) is a measure of the yielding

and the mobilized friction. This effect also appears in Figure II-18 when UTFSM and RAPEL records are used. As PGA increases, longer the period lengthening due to the significant nonlinearity of soil behavior.

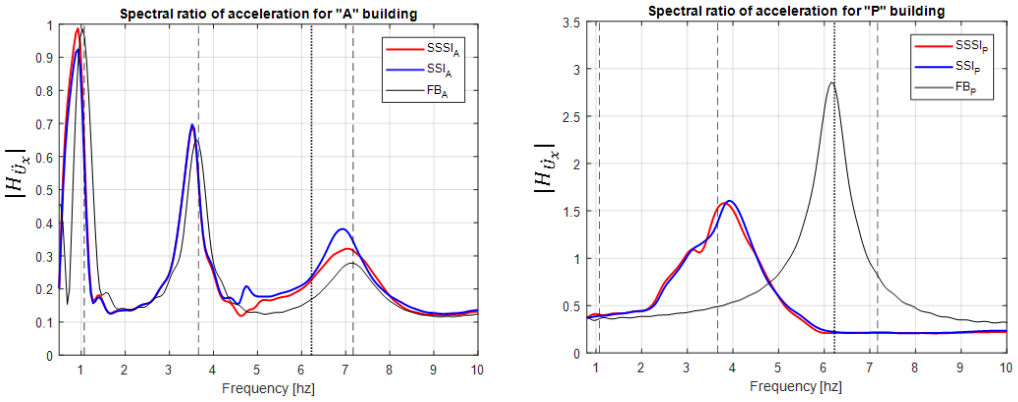

Figure II-17. Spectral ratio amplitude for the three scenarios: (a) "A" building and (b) "P" buildings. Fixed-base vibration frequencies are shown by dashed and dotted lines, respectively. Ricker of 5 Hz and outcropping amplitude of 0.10g.

Table II-4. Ratio of periods of vibration for case 5 Hz – 0.10g.

	T_{SSI}/T_{FB}		
	1st Mode	2nd Mode	3rd Mode
"A" building	1.10	1.03	1.03
"P" building	1.57	-	-

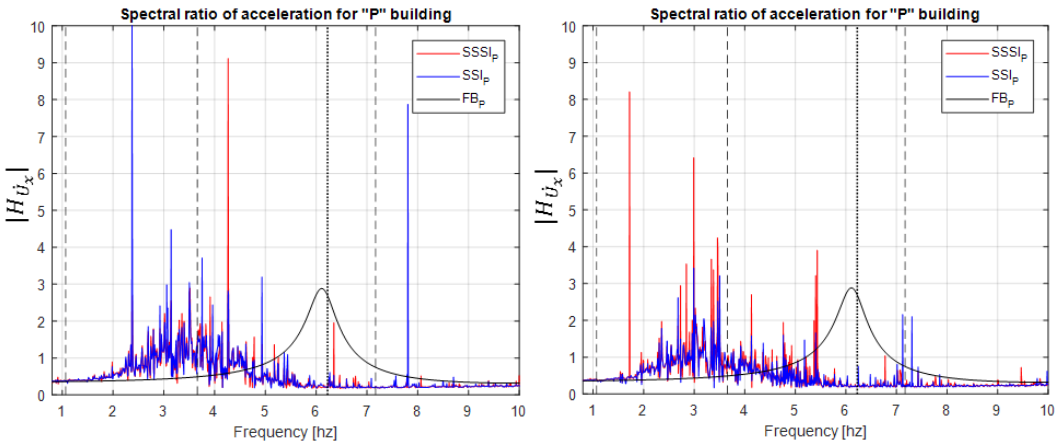

Figure II-18. Spectral ratio amplitude for the three scenarios and "P" building. (a) UTFSM record. (b) RAPEL seismic. Fixed-base vibration frequencies of both "A" and "P" buildings are shown by dashed and dotted lines, respectively.

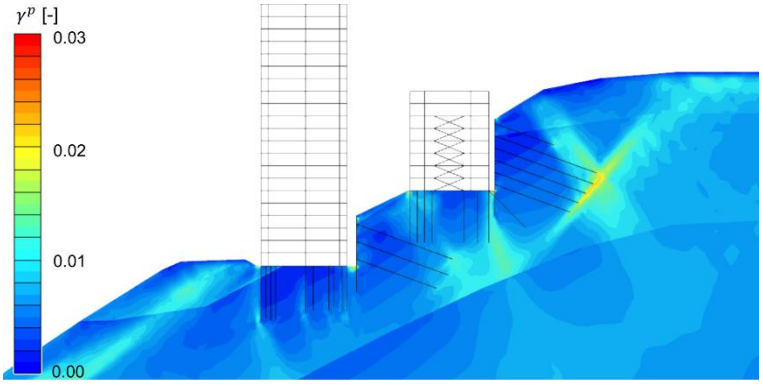

Figure II-19. Field of accumulated plastic deviatoric strain (γ^p) for the last load step of dynamic analysis.

Finally, the second spectral ratio for horizontal and vertical acceleration are shown in Figure II-20. The first scenario (top) shows the topographical amplification effects due to the excavation in the frequency domain discussed in section II.4.1. Also, the vertical ratio of this scenario shows that the excavation reduces the vertical acceleration

amplitudes (blue color) because more stiff sand appears close to the new ground level. The second scenario (bottom) shows SSI has a significant role in the reduction of high frequencies amplitudes ($f > 3\,Hz$) of vertical acceleration due to the kinematic constraint that the pile and micropile foundations impose on the foundation soil and probably because the additional confinement provided by the building's weight. However, the vertical ratio increases for low frequencies where the building's added mass to the system.

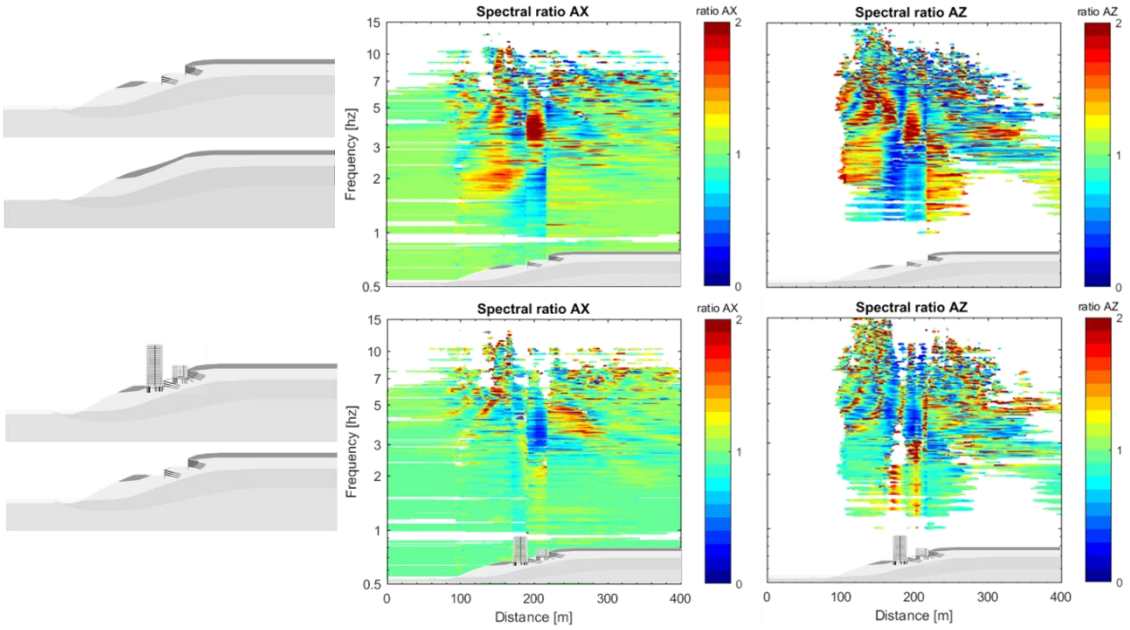

Figure II-20. Spectral ratio amplitudes for UTFSM seismic record. Left panel: Scenarios considered for the ratios. Central panel: Horizontal acceleration ratios. Right panel: Vertical acceleration ratios. The ratios have white color in zones where acceleration have a very low amplitude to avoid almost zero by zero quotients.

II.5 Conclusions

The dynamic nonlinear structure-soil-structure interaction for typical residential projects on coastal scarp were studied, a full structural models of 28-story apartment building and 8-story parking building were considered to develop an equivalent 2D-plane strain model including both structures and heterogenous site features. Ricker wavelet and seismic records were used as inputs. The lack of code provisions for slope-like topographical profile of coastal scarp were the main motivation of this study. The main findings are:

- Topographic profile as well as excavated surface profile have large effect on wave propagation patterns such as local zones in which motion are amplified or deamplified for specific frequencies i.e. TAF up to 2, VAF up to 1. Furthermore, using the TAF suggested in Eurocode 8 (EC8) could be unconservative for a maximum of about 43% for this case study. Also, these surface profiles can drastically change the kinematic of the motion of the considered low-rise building with period lengthening of 57%.
- Stratigraphy can modify the direction of propagation of waves reducing or amplifying the TAF and VAF in zones along the soil surface.
- Deep foundations enhance coupled responses of soil and structures, and they tend to decrease vertical acceleration component for high frequencies.
- Consideration of SSI analysis can reveal that base-fixed models for stiff low-rise buildings can lead to detrimental predictions of responses such as “P” building that presented amplification of interstory drift up to 80% and seismic coefficient up to 35% for some central frequencies of the Ricker pulses.

However, it is conservative for other frequencies and characteristic far-field seismic records.

- Additional effects of SSSI on structural responses was negligible for this specific case of study from a practical point of view.
- Interpreting results in terms of frequency and wavelength give a better quantitative understanding and insight of topographical effects and complex dynamic nonlinear soil-structure interaction phenomena.
- Similar residential projects on coastal scarp should take care of design of low-rise buildings located behind deep excavation and near slope crest.

II.6 Acknowledgments

This study is based upon work supported partially by the project FONDECYT 1200324 and partially by CIGIDEN (National Research Center of Integrated Natural Disaster Management) FONDAP 15110017. Also, the authors would like to acknowledge PRONABEC-Perú for providing a master degree studies scholarship to the first author under the supervision of the second author.

BIBLIOGRAFIA

ALAMO, G., PADRÓN, L., AZNÁREZ, J., MAESO, O. (2015) Structure-Soil-Structure Interaction Effects on the Dynamic Response of Piled Structures under Obliquely Incident Seismic Shear Waves. Soil Dynamics and Earthqueake Engineering, Vol. 78, p.142-153.

ALITALESH, M., SHAHNAZARI, H., HASSAN, M. (2018) Parametric Study on Seismic Topography-Soil-Structure Interaction; Topographic Effect. Geotechnical and Geological Engineering, Vol. 36, N°4, 2649-2666.

ASCE 7 (2017) Minimum Design Loads and Associated Criteria for Buildings and Other Structures. ASCE/SEI 7-16, Reston, VA.

ASSIMAKI, D., KAUSEL, E., GAZETAS, G. (2005) Wave Propagation and Soil-Structure Interaction on a Cliff Crest during the 1999 Athens Earthquake. Soil Dynamics and Earthquake Engineering, Vol. 25, N° 7-10, 513-527.

ASSIMAKI, D., MOHAMMADI, K. (2018) On the complexity of Seismic Waves Trapped in Irregular Topographies. Soil Dynamics and Earthquake Engineering, Vol. 114, 424-437.

ASSIMAKI, D., KAUSEL, E. (2007) Modified Topographic Amplification Factors for a Single-Faced Slope due to Kinematic Soil-Structure Interaction. Journal of Geotechnical and Geoenvironmental Engineering, Vol. 133, N°11, 1414-1431.

BENZ, T. (2007) Small-Strain Stiffness of Soils and its Numerical Consequences. Ph.D. Thesis. Institut für Geotechnik, Universität Stuttgart. Germany.

BOLISETTI, C., WHITTAKER, A. (2020) Numerical Investigations of Structure-Soil-Structure Interaction in Buildings. Engineering Structures, Vol. 215, 110709.

BORBON, F., DOMIZIO, M., AMBROSINI, D., CURADELLI, O. (2020) Influence of Various Parameters in the Seismic Soil-Structure Interaction Response of a Nuclear Power Plant. Engineering Structures, Vol. 217, 110820.

BOUCKOVALAS, G., PAPADIMITRIOU, A. (2005) Numerical Evaluation of Slope Topography Effects on Seismic Ground Motion. Soil Dynamics and Earthquake Engineering, Vol. 25, 547-558.

CHOINIERE, M., PAULTRE, P., LÉGER, P. (2019) Influence of Soil-Structure Interaction on Seismic Demands in Shear Wall Building Gravity Load Frames. Engineering Structures, Vol. 198, 109259.

COMTE, D., EISENBERG, A., LORCA, E., PARDO, M., PONCE, L., SARAGONI, R., SINGH, S., SUAREZ, G. (1986) The 1985 central Chile earthquake: A repeat of previous great earthquakes in the region?, Science, Vol. 233, N° 4762, 449-453.

COOLEY, J., TUKEY, J. (1965) An algorithm for the machine calculations of complex Fourier series. Mathematics of Computation, Vol. 19, N° 90, 297-301.

DAO, T. (2011) Validation of PLAXIS Embedded Piles For Lateral Loading. Ph.D. Thesis. Faculty of Civil Engineering and Geosciences, Delft University of Technology.

DE SOUZA NETO, E., PERIC, D., OWEN, D. (2011) Computational methods for plasticity: theory and applications. John Wiley & Sons.

DI FIORE, V. (2010) Seismic Site Amplification Induced by Topographic Irregularity: Results of a Numerical Analysis on 2D Synthetic Models. Engineering Geology, Vol. 114, 109-115.

EUROCODE 8 (EC8) (2004) Design of Structures for Earthquake Resistance – Part 5: Foundations, Retaining Structures and Geotechnical Aspects. BS EN 1998-5:2004

HAN, B., CHEN, S., LIANG, J. (2020) 2D Dynamic Structure-Soil-Structure Interaction: A Case Study of Millikan Library Building. Engineering Analysis with Boundary Elements, Vol. 113, 346-358.

KAUSEL, E. (2010) Early History of Soil-Structure Interaction. Soil Dynamics and Earthquake Engineering, Vol. 30, N° 9, 822-832.

KAUSEL, E. (2006) Fundamental Solutions in Elastodynamics: A Compendium. Cambridge University Press.

LUCO, E., CONTESSE, L. (1973) Dynamic Structure-Soil-Structure Interaction. Bulletin of the Seismological Society of America, Vol. 63 N° 4, 1289-1303.

MENGLIN, L., HUAIFENG, W., XI, C., YONGMEI, Z. (2011) Structure-Soil-Structure Interaction: Literature Review. Soil Dynamics and Earthquake Engineering, Vol. 31, N° 12, 1724-1731.

MIKKELSEN, P. (2003) Advances in Inclinometer Data Analysis. Symposium on Field Measurements in Geomechanics. Oslo.

MYLONAKIS, G., GAZETAS, G. (2000) Seismic Soil-Structure Interaction: Beneficial or Detrimental?. Journal of Earthquake Engineering, Vol. 4, N° 3, 277-301.

NGUYEN, K., GATMIRI, B. (2007) Evaluation of seismic Ground Motion Induced by Topographic Irregularity. Soil Dynamics and Earthquake Engineering, Vol. 27, N° 2, 183-188.

NTCS-17 (2017) Normas Técnicas Complementarias para Diseño por Sismo, Gaceta Oficial de la Ciudad de México, N°. 220-BIS, diciembre.

PAOLUCCI, R. (2002) Amplification of Earthquake Ground Motion by Steep Topographic Irregularities. Earthquake Engineering and Structural Dynamics, Vol. 31, N° 10, 1831-1853.

PAPAGEORGIOU, A., KIM, J. (1991) Study of the Propagation and Amplification of Seismic Waves in Caracas Valley with Reference to the 29 July 1967 Earthquake: SH Waves. Bulletin of the Seismological Society of America, Vol. 81, N° 6, 2214-2233.

PLAFKER, G., SAVAGE, J. (1970) Mechanism of the Chilean earthquakes of May 21 and 22, 1960. Geological Society of America Bulletin, Vol. 81, N° 4, 1001-1030.

PLAXIS, Plaxis2D-Reference Manual, CONNECT Edition V20.02, 2020.

POURSARTIP, B., FATHI, A., KALLIVOKAS, L. (2017) Seismic Wave Amplification by Topographic Features: A Parametric Study. Soil Dynamics and Earthquake Engineering. Vol. 92, 503-527.

RADDATZ, D., TAIBA, O. (2018) Estructura de Contención usando Pilas con Anclajes y Refuerzo de Fundaciones por Medio de Micropilotes y Pilas para Proyecto Ubicado en Reñaca, Viña del Mar. X Congreso SOCHIGE, 3, 4 y 5 de Diciembre. Valparaiso.

RATHJE, E., ABRAHAMSON, N., BRAY, J. (1998) Simplified Frequency Content Estimates of Earthquake Ground Motions. Journal of Geotechnical and Geoenvironmental Engineering, Vol. 124, N° 2, 150-159.

ROESSET, J. (2013) Soil Structure Interaction The Early Stages. Journal of Applied Science and Engineering, Vol. 16, N° 1, 1-8.

SAEZ, E. (2009) Dynamic nonlinear soil-structure interaction. Doctoral dissertation. Ecole Centrale Paris.

SCHAFER, R., RABINER, L. (1973) Design and Simulation of Speech Analysis-Synthesis System Based on Short-Time Fourier Analysis. IEEE Transactions on Audio and Electroacoustics. Vol. 21, N° 3, 165-174.

SCHANZ, T., VERMEER, P., BONNIER, P. (1999) The hardening soil model: formulation and verification. Beyond 2000 in computational geotechnics, 281-296.

SEMBLAT, J.F., PECKER, A. (2009) Waves and Vibration in Soils: Earthquakes, Traffic, Shocks, Construction works. IUSS Press.

SIMO, J., HUGHES, T. (2006) Computational Inelasticity. Springer Science & Business Media.

SLUIS, J., BESSELING, F., STUURWOLD, P., LENGKEEK, A. (2013) Validation and Application of the Embedded Feature in PLAXIS 2D. Plaxis Bulletin. Vol. 34, 10-13.

TADEU, A., SANTOS, P, ANTÓNIO, J. (2001) Amplification of Elastic Waves due to a Point Source in the Presence of Complex Surface Topography. Computers and Structures, Vol. 79, N° 18, 1697-1712.

TADMOR, E., MILLER, R., ELLIOTT, R. (2012) Continuum mechanics and thermodynamics: from fundamental concepts to governing equations. Cambridge University Press.

UDIAS, A., MADARIAGA, R., BUFORN, E., MUÑOZ, D., ROS, M. (2012) The large Chilean historical earthquakes of 1647, 1657, 1730, and 1751 from contemporary documents. Bulletin of the Seismological Society of America, Vol. 102, N° 4, 1639-1653.

UGALDE, D., LOPEZ-GARCIA, D. (2020) Analysis of the Seismic Capacity of Chilean Residential RC Shear Wall Buildings. Journal of Building Engineering, Vol. 31, 101369.

VICENCIO, F., ALEXANDER, N. (2018) Higher Mode seismic Structure-Soil-Structure Interaction between Adjacent Building during Earthquakes. Engineering Structures, Vol. 174, 322-337.

VICENCIO, F., ALEXANDER, N. (2019) Dynamic Structure-Soil-Structure Interaction in Unsymmetrical Buildings due to Seismic Excitation. Soil Dynamics and Earthquake Engineering, Vol. 127, 105817.

WESTENENK, B., DE LA LLERA, J., JÜNEMANN, R., HUBE, M., BESA, J., LÜDERS, C., INAUDI, J., RIDDELL, R., JORDÁN, R. (2013) Analysis and Interpretation of the Seismic Response of RC Buildings in Concepción During The February 27, 2010, Chile Earthquake. Bulletin of Earthquake Engineering, Vol. 11, N° 1, 69-91.

WOLF, J. (1985) Dynamic Soil-Structure Interaction. Prentice-Hall, Inc., Englewood Cliffs, New Jersey.

WONG, H., TRIFUNAC, M. (1975) Two-Dimensional, Antiplane, Building-Soil-Building Interaction for Two or More Buildings and for Incident Plane SH

Waves. Bulletin of the Seismological Society of America, Vol. 65, N° 6, 1863-1885.

ZHANG, Z., FLEURISSON, J., PELLET, F. (2018) The Effects of Slope Topography on Acceleration Amplification and Interaction Between Slope Topography and Seismic Input Motion. Soil Dynamics and Earthquake Engineering, Vol. 113, 420-431

ZIENKIEWICZ, O., CHAN, A., PASTOR, M., SCHREFLER, B., SHIOMI, T. (1999) Computational Geomechanics with Special Reference to Earthquake Engineering. John Wiley & Sons Ltd., England.

A N E X O S

ANEXO A : EJEMPLO DE *SCRIPT* EN LENGUAJE PYTHON PARA AUTOMATIZAR EXTRACCIÓN DE RESULTADOS DE PLAXIS2D®

El siguiente script en Python muestra un sencillo ejemplo de código para vincular Python con Plaxis2D® v20, modificar un modelo existente y extraer resultados específicos en formato de texto.

```
# Extraer resultados de varios Rickers, funciona con modelo parcialmente construido
# Julio César Sucasaca Rodríguez
# jcsucasaca@uc.cl
# 2020
# ============================================================================================
import numpy as np
from plxscripting.easy import new_server
s_i, g_i = new_server('localhost', 10000, password='M@=siv3r4xW#u%6~')
from plxscripting.easy import new_server
s_o, g_o = new_server('localhost', 10001, password='M@=siv3r4xW#u%6~')

# ============================================================================================
NroPuntos = 192 # Puntos de output
f=5             # Frecuencia central del pulso Ricker
fmesh = 10      # Frecuencia para mallar
# ============================================================================================
fmax = 4    # Frecuencia minima que ve la malla para todos los analisis
vs = 300    # Vs de estrato mas critico [m/s]
lamb = vs/f # longitud de onda [m]
# ============================================================================================
# Script 1 al 4 para copiar y correr individualmente en Interpreter, luego correr este
script mientras se va por un café :)
# ============================================================================================

# 1. AMORTGUAMIENTO MATERIAL EN FUNCION DE f
#============================================
def Material_AmortRayleigh(f):
# para ver los 15 estratos:
# for i in [0,1,2,3,4,5,6,7,8,9,10,11,12,13,14,15]:
# print(str(i) +': '+ g_i.Materials[i].Name.value)

    # ESTRATOS  ============
    xi = 3  # Amortiguamiento en %
    alpha = 0.06222*xi*f # regresion practica
    beta = 0.001473*xi/f
    for i in [0, 1, 2, 3, 4,5,6,7,8,9,10,11]:
        g_i.Materials[i].setproperties("RayleighAlpha", alpha, "RayleighBeta", beta)

    # COLUMNAS LATERALES ============
    xi = 12  # Amortiguamiento en %
    alpha = 0.06222*xi*f
    beta = 0.001473*xi/f
```

```
    for i in [12, 13,14,15,16]:
        g_i.Materials[i].setproperties("RayleighAlpha", alpha, "RayleighBeta", beta)
# 2. OBJETOS PUNTOS EN SUPERFICIE DE TALUD QUE SERVIRAN DE GUIA PARA FUNCION 4
#=======================================
def Guia_Mesh():
    #~ # Acceeder mediante Puntos en Structures(), Geometry/Points/LabelNumber

    Etiqueta_de_nodos = [6, 47, 54, 1] # nodos que definen el talud simplificado
    PuntoName = []
    Xlist = []
    Ylist = []
    g_i.gotostructures()
    for i in Etiqueta_de_nodos:
        count = 0
        for point in g_i.Points:
            if point.Name.value == 'Point_'+str(i):
                PuntoName.append(g_i.Points[count].Name.value)
                Xlist.append(g_i.Points[count].x.value)
                Ylist.append(g_i.Points[count].y.value)
            count = count + 1
    return Xlist, Ylist

# 3. GENERAR MALLA
#=======================================
def Mesh(fmesh, fmax, vs):
    meshsize = min(vs/fmesh/8, 311/fmax/8)*2 # 16 nodos por long de onda
    g_i.gotomesh()
    a = g_i.meshd(meshsize)
    print(a)

# 4. SELECCIONAR PUNTOS PRE-CALC
#=======================================
def PreCalc(Xlist, Ylist, lamb, vs, fmax, NroPuntos):
    g_i.gotomesh()
    print("Nro de puntos para curvas: " +str(NroPuntos))
    XlistPre = []
    YlistPre = []
    g_i.selectmeshpoints()
    Xsurface = np.linspace(-50, 450, num=NroPuntos, endpoint=True)
    count = 1
    for Xsur in Xsurface:
        Ysur = np.interp(Xsur, Xlist, Ylist)
        g_o.addcurvepoint('node', (Xsur, Ysur), (-1, -0.5))
        print(g_o.Nodes[-1].Name.value +" " + str(count))  # para ver curvepoint
        count = count +1
    for i in np.arange(len(Xsurface)):
        XlistPre.append(g_o.Nodes[int(i)].x.value)
        YlistPre.append(g_o.Nodes[int(i)].y.value)
    g_o.update()

    return Xsurface, XlistPre, YlistPre
```

```
# Correr en interpreter uno a uno para actualizar el modelo para el Ricker que se usará:
#~ Material_AmortRayleigh(f)
#~ Xlist, Ylist = Guia_Mesh()
#~ Mesh(fmesh, fmax, vs)
#~ Xsurface, XlistPre, YlistPre = PreCalc(Xlist, Ylist, lamb, vs, fmax, NroPuntos)
# Analizar el modelo manualmente

# Exportar datos de curvas de aceleración en X versus tiempo (u otros)
# ==============================
def CurvasVst(start_s, start_n, XlistPre, YlistPre):
    g_i.save()
    filenamelog= r'F:\TESIS\logAnalisisTesisCurves.txt'
    filename= r'F:\TESIS\Ampli_topo_curve_est_f0_15_AX.txt'  # cambiar nombre

    # Solo para primera exportacion (antes de que suceda el error Json)
    if start_s == 0 and start_n == 0:
        with open(filename, "w") as file:
            file.writelines(["Step"+"\t"+"Step"+"\t"+"Dyn_time"+"\n"])

            # Exporto coordenadas X
            file.writelines([" "+"\t"+" "+"\t"+" "])
            for i in np.arange(len(XlistPre)):
                if i == np.arange(len(XlistPre))[-1]:
                    file.writelines(["\t" + str(XlistPre[i]) + "\n"])
                else:
                    file.writelines(["\t" + str(XlistPre[i]) ])

            # Exporto coordenadas Y
            file.writelines([" "+"\t"+" "+"\t"+" "])
            for i in np.arange(len(YlistPre)):
                if i == np.arange(len(YlistPre))[-1]:
                    file.writelines(["\t" + str(YlistPre[i]) + "\n"])
                else:
                    file.writelines(["\t" + str(YlistPre[i]) ])

            # Primera fila de tiempo cero con valores cero
            file.writelines([str(0)+"\t"+str(0) + "\t" + str(0) ])
            for i in np.arange(len(XlistPre)):
                if i == np.arange(len(XlistPre))[-1]:
                    file.writelines(["\t" + str(0) + "\n"])
                else:
                    file.writelines(["\t" + str(0) ])
            file.close()
    else:
        start_n = start_n + 1 #  siguiente nodo
    nnn = [x for x in g_o.Nodes]
    nnn = nnn[0:len(XlistPre)]   # excluyo nodos PreCalc manuales
    sss = [y for y in g_o.Phase_1.Steps]
    sss = sss[1::2] # para tener STEPS 15, 17, 19, ..., 613
    for i in np.arange(start_s, len(sss)):
        step = sss[i]
        dyntime = step.Reached.DynamicTime.value
```

```
        for j in np.arange(start_n, len(nnn)):
            node = nnn[j]
            if j == 0:
                with open(filename, "a") as file:
                    file.writelines([str(i)+"\t"+str(i) + "\t" + str(dyntime) ])
            AX = g_o.getcurveresults(node, step, g_o.ResultTypes.Soil.Ax)/2 # just incoming
wave
            if j == np.arange(len(nnn))[-1]:
                with open(filename, "a") as file:
                    file.writelines(["\t" + str(AX) + "\n"])
            else:
                with open(filename, "a") as file:
                    file.writelines(["\t" + str(AX) ])

            # Guardo en archivo logAnalisisTesisCurves.txt el ultimo nodo que exporto
            with open(filenamelog, "w") as filelog:
                if j == np.arange(start_n, len(nnn))[-1]:
                    start_n = 0
                    filelog.writelines([str(i) + "\n" + str(0)]) # step y nodo
                else:
                    filelog.writelines([str(i) + "\n" + str(j)]) # step y nodo
                filelog.close()
        print(str(step.Name.value))

# ========================
# SCRIPT (funciona luego de correr y guardar el modelo)
# Además, considera la posible ocurrencia de un error de compilación (…Json…)
# por lo que es necesario guardar en un archivo de texto "filelog" los datos de
# los últimos datos exportados con éxito. Lo que agrande este código
# ========================
XlistPre = []
YlistPre = []
for i in np.arange(NroPuntos):
    XlistPre.append(g_o.Nodes[int(i)].x.value)
    YlistPre.append(g_o.Nodes[int(i)].y.value)
while True:
    filenamelog= r'F:\TESIS\logAnalisisTesisCurves.txt'
    filelog = open(filenamelog,"r")
    start_s = filelog.readline()
    start_s = int( start_s.replace("\n","") )
    start_n = int(filelog.readline())
    filelog.close()
    try:
        CurvasVst(start_s, start_n, XlistPre, YlistPre)
        break
    except:
        print('Sucedio el error Json', "\n", 'Continuado Exportacion de resultados')
# Reinicio filenamelog a cero
with open(filenamelog, "w") as filelog:
    filelog.writelines([str(0) + "\n" + str(0)])
    filelog.close()
print("finish", "\n", '='*29)
```